OPTIMAL ELECTRIC POWER TAKE-OFF STRATEGY FOR SURFACE RIDING

WAVE ENERGY CONVERTERS

A Thesis

by

SHRIKESH SHESHAPRASAD

Submitted to the Graduate and Professional School of
Texas A&M University
in partial fulfillment of the requirements for the degree of

MASTER OF SCIENCE

Chair of Committee,	Hamid A. Toliyat
Committee Members,	Prasad Enjeti
	Shankar P. Bhattacharyya
	HeonYong Kang
Head of Department,	Miroslav Begovic

May 2022

Major Subject: Electrical Engineering

ABSTRACT

Wave energy has been proven to be a significant source of renewable energy. The surface riding wave energy converter (SR-WEC) is a novel approach to capturing wave energy in small and intermediate scales. This approach uses a tube-like structure housing a permanent magnet tubular linear generator to convert the kinetic energy of the sliding magnet assembly into electrical energy. The motion of the magnet assembly is dictated by the excitation forces from the ocean waves.

The power capture from the linear generator is controlled by the power take-off (PTO) strategy. This study investigates the use of traditional PTO strategies such as passive, reactive PTO for the SR-WEC. Novel binary and binary-reactive PTOs are proposed. These novel strategies are best suited for use in the SR-WEC. A parametric optimization process for each PTO strategy is discussed.

The study also explores the design and optimization of a permanent magnet linear generator for use in the SR-WEC with low cost being the driving factor in order to keep the minimum levelized cost of energy. The design and fabrication of a small scale prototype is discussed. The challenges associated with the linear generator fabrication and use is a point of interest in this study.

DEDICATION

To my parents: *Roopa and Prasad*

ACKNOWLEDGEMENTS

CONTRIBUTORS AND FUNDING SOURCES

Contributors

NOMENCLATURE

PTO   Power Take-Off

WEC   Wave Energy Converter

SR-WEC   Surface Riding Wave Energy Converter

PM   Permanent Magnet

PMTL   Permanent Magnet Tubular Linear

C_{PTO} Viscous Damping Coefficient

K_{PTO} Stiffness Coefficient

X_{rel} Position of Translator

$\dot{X}_{rel}$ Speed of Translator

F_{PTO} Power Take-off Force

AEP   Annual Energy Production

LCOE   Levelized Cost of Energy

FEA   Finite Element Analysis

TROMAG   Trans-Rotary Magnetic Gear

FOC   Field Oriented Control

TABLE OF CONTENTS

LIST OF FIGURES

LIST OF TABLES

1. INTRODUCTION

The energy demand in today's world is constantly rising. The dependence on traditional sources of energy is increasing the financial burden for most countries as well as impacting the environment in an irreversible manner. In order to overcome this negative impact, there is a need for clean, renewable sources of energy at affordable cost. One renewable source is the ocean waves. Ocean waves contain a substantial amount of energy. Waves are generated as a result of winds blowing on the ocean surface. These winds are caused by the redistribution of solar energy. Waves can build up over time and reach energy densities averaging over 100 *kW/m*. The highest annual average energy density of >140 *kW/m* is found at 48°S, 90°E which is about 1400 *km* east of Kerguelen Island in the Indian Ocean [1]. However, locations such as these are very remote and the cost of installing and operating an energy conversion system is economically not feasible. Some estimates show that it is technologically feasible to harvest approx. 6% of the national energy demand of the U.S from the wave energy that reaches its coastline [2]. In order to make use of the abundant energy available in the ocean, several wave energy converters have been explored. Wave energy converters (WEC) were conceptualized as early as 1799 [3]. According to a review in 2015, there were at least 170 WECs in various stages of development [4].

1.1 Wave energy converter technologies and challenges

Capturing energy from the ocean waves poses several challenges. The device needs to be able to operate in the harsh conditions of open ocean, withstand extreme forces

during storms and not require maintenance for extended periods of time. In order to compete with conventional energy sources, the WEC system needs to be cost efficient to capture energy at an economical levelized cost of energy (LCOE). The converter needs to transfer the power to a location where it is usable. Most WECs convert wave energy into electricity. This requires the use of long transmission cables which adds to the LCOE. Thus, it is indeed a challenge to design a WEC that suits all these conditions. Several wave energy conversion systems have been discussed in [5-8]. These WECs can be broadly classified into three groups: oscillating water columns, overtopping devices and oscillating bodies. The basic structures of these groups are shown in Figure 1
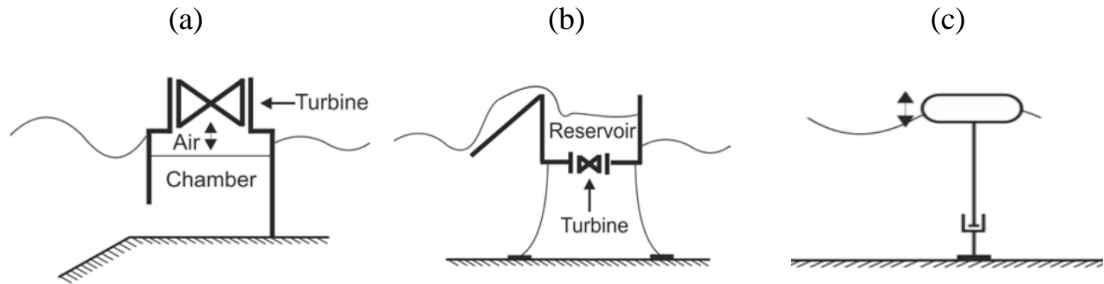
Figure 1: WEC types a) Oscillating water column b) Overtopping device c) Oscillating body

1.1.1 Oscillating water columns

The basic structure of an Oscillating water column type WEC is shown in Figure 1a. They use the ocean waves to press air through an air turbine. When an ocean wave hits the device, the water level inside the chamber rises pressing the air. When the wave retracts, the air come back into the chamber again through the turbine [9].

2

1.1.2 Overtopping devices

An overtopping device type WEC has a water reservoir which can be floating or fixed as shown in Figure 1b. When the ocean waves hit the device, water spills into the reservoir. The excess potential energy of the water in the tank is discharges through a turbine thus generating electricity [10].

1.1.3 Oscillating bodies

Oscillating body type WECs can be floating, fixed or submerged. These devices use the wave motion to capture the kinetic energy of the incidental waves. A simple example is shown in Figure 1c. These bodies have pitch, roll, yaw, heave, sway and surge motions.

1.1.4 Surface riding wave energy converter

The recently invented surface riding wave energy converter (SR-WEC) [11] provides a new approach to competitively convert wave energy to renewable electricity in small or intermediate scales. The SR-WEC consists of an outer cylinder housing a permanent magnet (PM) linear generator that has a stator made of copper windings and a PM translator sliding on a center rod as seen in Figure 2. This apparatus rides on the surface of the ocean waves and is pitched up and down as the wave elevation changes. As the wave elevation (θ_{wave}) changes, the translator is pushed across the length of the tube. The translator experiences a force:

$$F_{excitation} = mg \sin \theta_{tube} \qquad (1)$$

where m is the mass of the translator, θ_{tube} is the elevation angle of the SR-WEC and g is the gravitational acceleration constant. This force accelerates the PM translator, and the resulting kinetic energy is harnessed through the windings of the linear generator.

The speed of the sliding mass can be found by using:

$$speed(x + 1) = speed(x) + \Delta t * (F_{excitation} + F_{PTO}) * g \qquad (2)$$

where, x is the current time interval, Δt is the time step of computation, and F_{PTO} is the PTO force which is discussed more in Chapter 2. Similarly, the position of the sliding mass can be estimated using:

$$position(x + 1) = position(x) + \Delta t * \frac{[speed(x) + speed(x + 1)]}{2} \qquad (3)$$

The relative invariance of the wave slopes throughout different sea states allows an inherently extended operating window in annual operation, and the rotational tilting motions make resonance control easier through relocating a mass [12]. To resonate the tilt motion with varying incident wave frequencies, movable rings in the buoyancy unit can be relocated such that the natural frequency of the tilt coincides with that of the incident wave. This gives the SR-WEC an advantage over other forms of WECs since it can extract energy from a wide range of incident wave frequencies. To ensure reliable long-term production with a simpler system [13], the PM linear generator is sealed inside the cylinder, which improves survivability beyond other existing wave energy converters with generation interfaces exposed to the ocean waves.
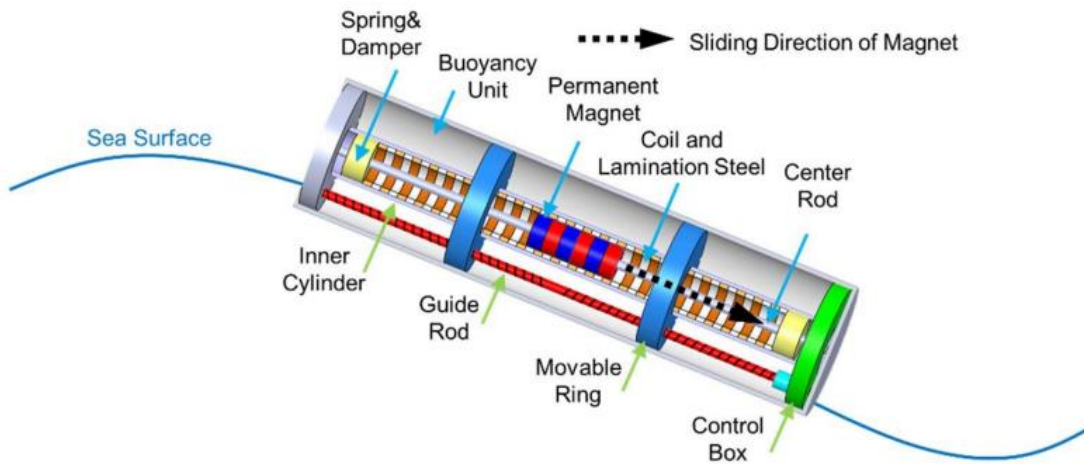
Figure 2: Surface Riding Wave Energy Converter

1.2 Overview of thesis

This thesis concerns a surface riding wave energy converter. Chapter 2 explores the various PTO strategies that exist for WECs and proposes a novel algorithm that suits best for the SR-WEC. Chapter 3 talks about the optimization of the PTO algorithms and contrasts their functioning based on a set of wave data. Chapter 4 discusses the design of a linear generator for use in the SR-WEC. A small-scale prototype is also discussed in Chapter 4. Chapter 5 deals with the experimental results of the different PTO algorithms. Finally, Chapter 6 summarizes the work and provides the future scope for research in this field.

2.   POWER TAKE-OFF IN WAVE ENERGY CONVERTERS

The power take-off (PTO) strategy is responsible for ensuring that the WEC is utilized in the most effective manner by extracting as much electrical energy from the waves as possible. Various PTO damping strategies are discussed in [14-16]. These include passive, reactive and discrete PTO strategies. The intensity and duration of force applied on the translator during energy harvesting is set by the PTO strategy. Thus, these strategies play an important role in determining the average output power generation as well as the generator specifications of the SR-WEC. The implementation of these PTO strategies can be carried out by using a control algorithm suitable for controlling the PM linear generator. A sensorless control algorithm is most suitable as the design objectives of the SR-WEC are very cost sensitive in order to keep the LCOE to a minimum. Several sensorless control mechanisms have been discussed in [17-20].

2.1 Passive PTO

One of the simplest forms of PTO is loading the SR-WEC passively. This replicates a simple viscous damping of the sliding motion. The force applied on the PM translator is directly proportional to its speed. The PTO force is given by:

$$F_{PTO} = -C_{PTO}\dot{X}_{rel},\tag{4}$$

Where F_{PTO} is the PTO force applied by the generator, C_{PTO} is the viscous damping coefficient, and $\dot{X}_{rel}$ is the speed of the sliding mass relative to the stator. While applying the F_{PTO} it is also important to ensure that the power and force limits of the system are not breached. The passive PTO force is shown in Figure 3 and the corresponding speed and position of the PM translator is shown in Figure 4. It can be seen that the force is directly

6

proportional to the speed of the PM translator. The passive PTO algorithm is explained in

Figure 5.
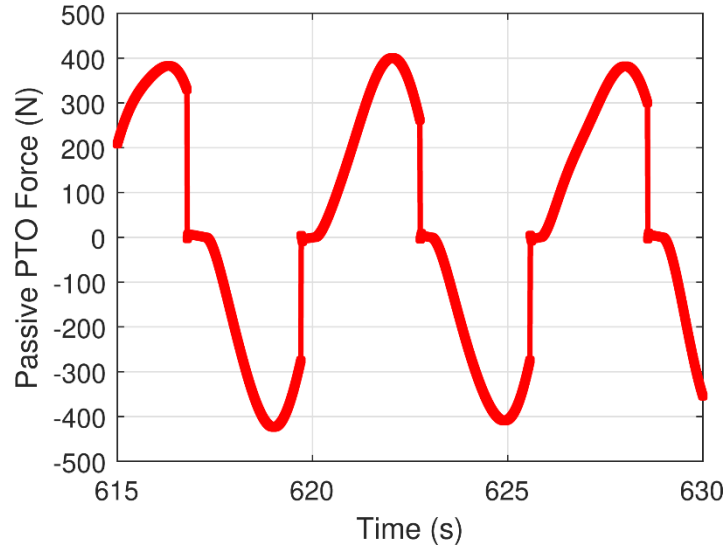
Figure 3: Passive PTO force profile
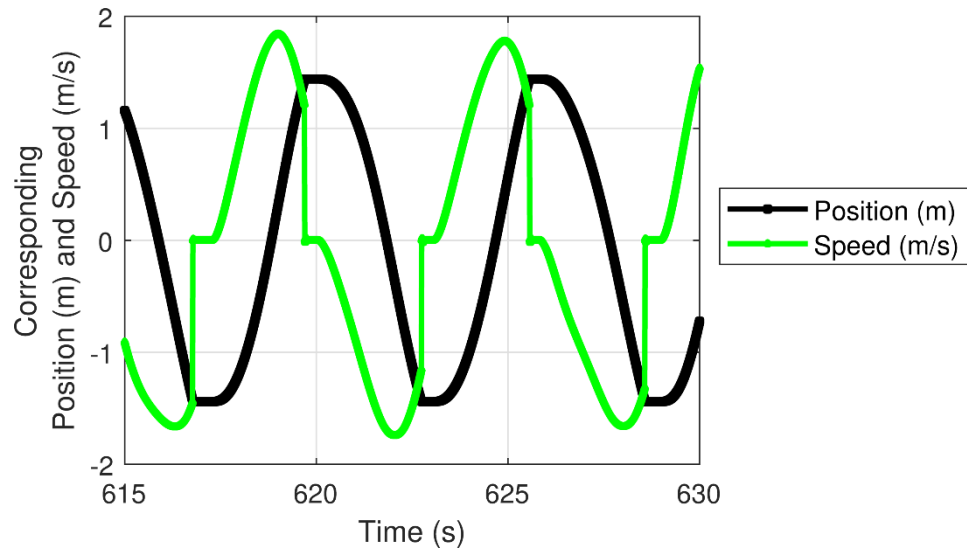
Figure 4: Passive PTO - Corresponding position and speed
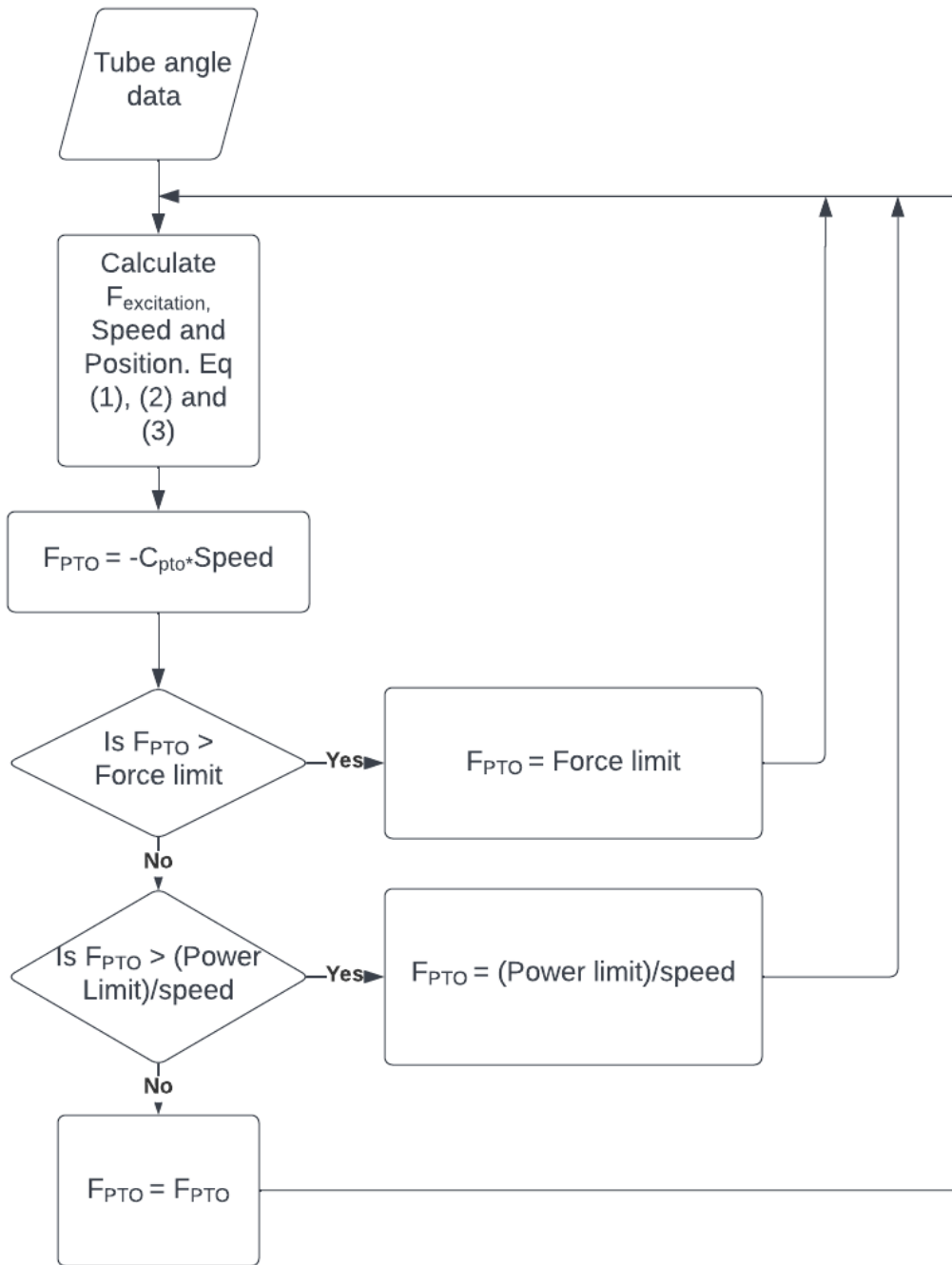
Figure 5: Passive PTO algorithm

2.2 Reactive PTO

Reactive PTO is where the PTO force has two components. One is proportional to the relative speed of the translator, and the other is proportional to the position. This replicates a viscous damper along with a stiffness spring. The reactive PTO for force is given by:

$$F_{PTO} = -K_{PTO}X_{rel} - C_{PTO}\dot{X}_{rel} \tag{5}$$

Where K_{PTO} is the stiffness coefficient and X_{rel} is the position of the sliding mass relative to the stator. Thus, the generator emulates both an electrical spring and an electrical viscous damper. If the impedance of the wave motion is matched by the impedance of the PTO stiffness coefficient, maximum power transfer can be achieved. Like in passive PTO, it is important to ensure that the force and power limits are not breached while applying the PTO force on the PM translator. The application of reactive PTO force is shown for a certain time interval in Figure 6. The corresponding speed and position of the PM translator is shown in Figure 7. It can be seen that the force is a function of both speed and position of the translator. The reactive PTO algorithm is explained in Figure 8.
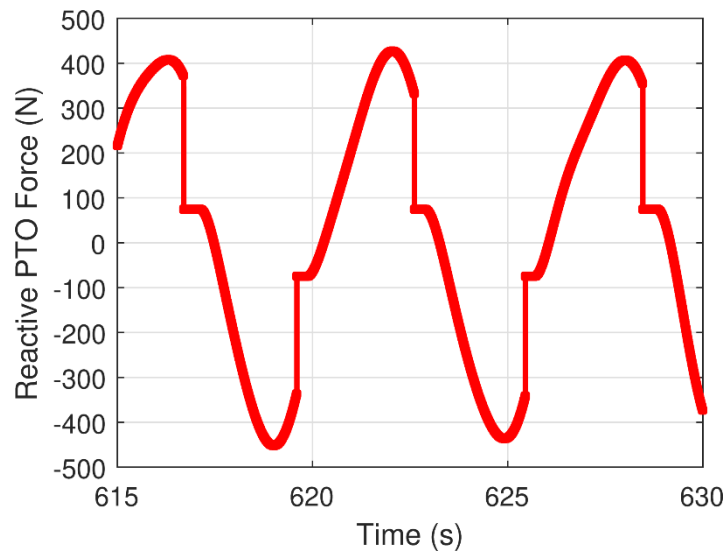
Figure 6: Reactive PTO force profile
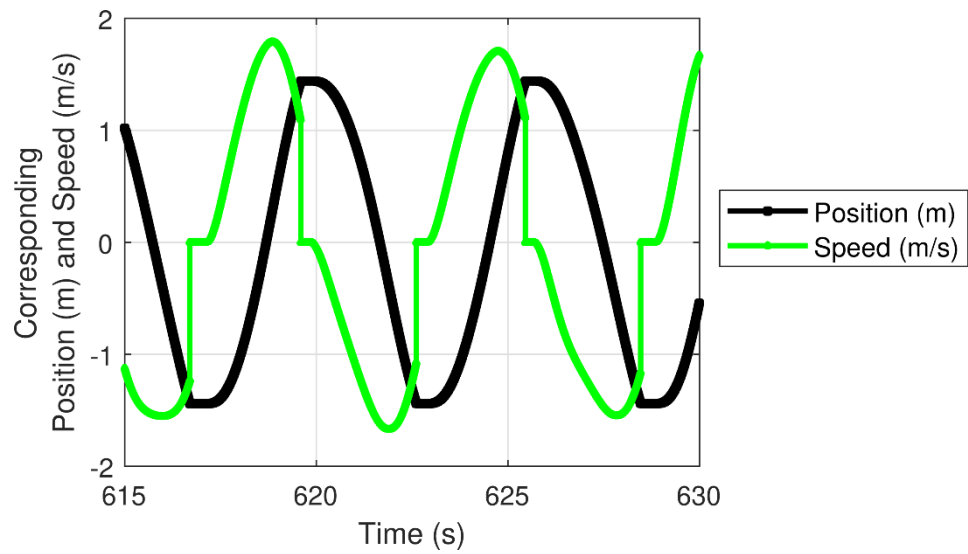
Figure 7: Reactive PTO - Corresponding position and speed

10
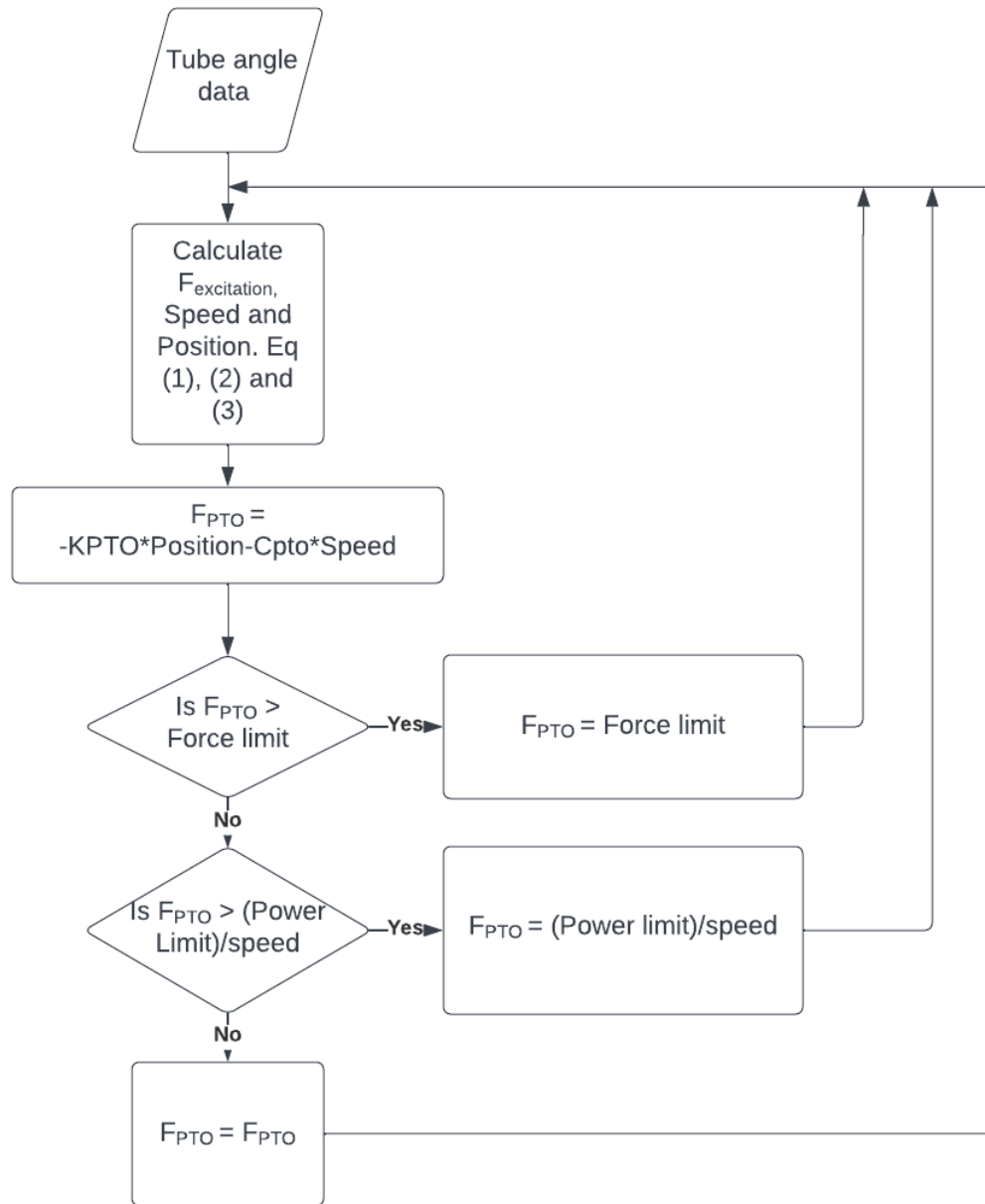
Figure 8: Reactive PTO algorithm

In a reactive PTO implementation, a bidirectional power flow is required between the DC bus and the linear generator. In order to effectively match the impedance of the PTO to that of the wave impedance, the K_{PTO} coefficient needs to be set according to (6).

$$K_{PTO} = slidingMass * \left(\frac{2\pi}{peakPeriod}\right)^2 \tag{6}$$

where, $slidingMass$ is the mass of the PM translator, and $peakPeriod$ is the peak period of the given wave. Typically, reactive PTO is seen to be the most optimal under the assumption of sinusoidal incident waves [14]. However, under irregular wave conditions, and the limited sliding distance in the SR-WEC, the reactive damping fails to provide the optimal PTO output.

2.3 Binary PTO

Binary PTO damping is a strategy where the generator is in either an ON or OFF state. Whenever the generator is ON, it generates the maximum instantaneous power, subject to its force and power ratings. This generator is turned ON whenever the sliding mass approaches the end of the tube or when the tube changes its direction of tilt such that the mass is sliding uphill. The generator is then turned off when the sliding mass is brought to a stop. A binary timing term called the *binary factor* is used to control how early or late the generator is turned ON before hitting the ends of the tube. The force profile of the binary PTO is shown in Figure 9 along with the position and speed values in Figure 10. It can be seen that as the translator reaches the ends of the tube, the generator is turned ON

to apply maximum force. The functioning of binary PTO algorithm is explained in Figure

11.
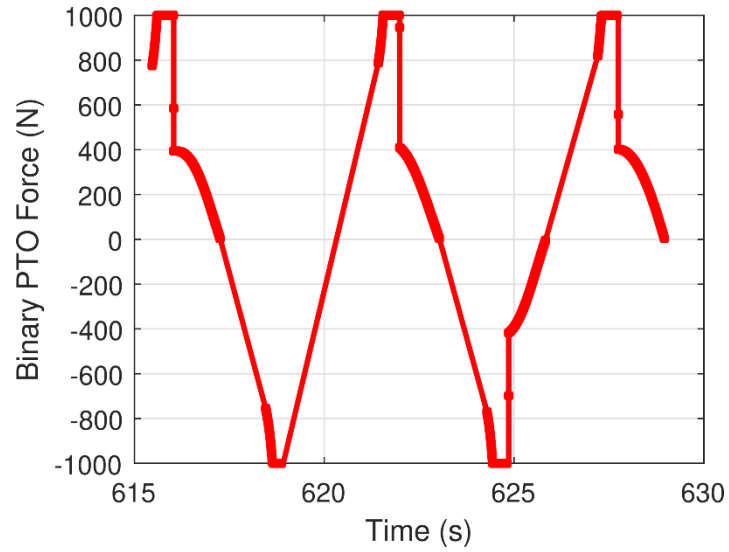
Figure 9: Binary PTO force profile
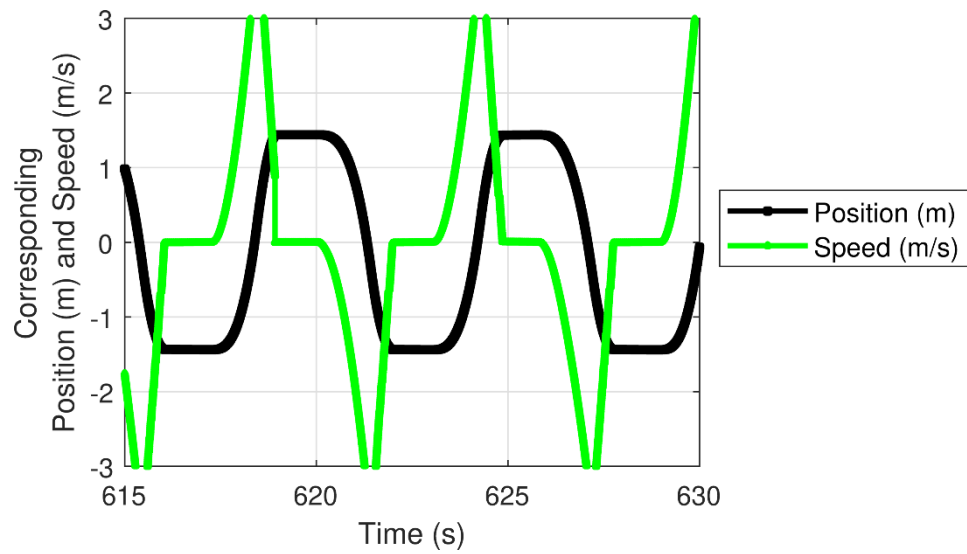
Figure 10: Binary PTO - Corresponding position and speed
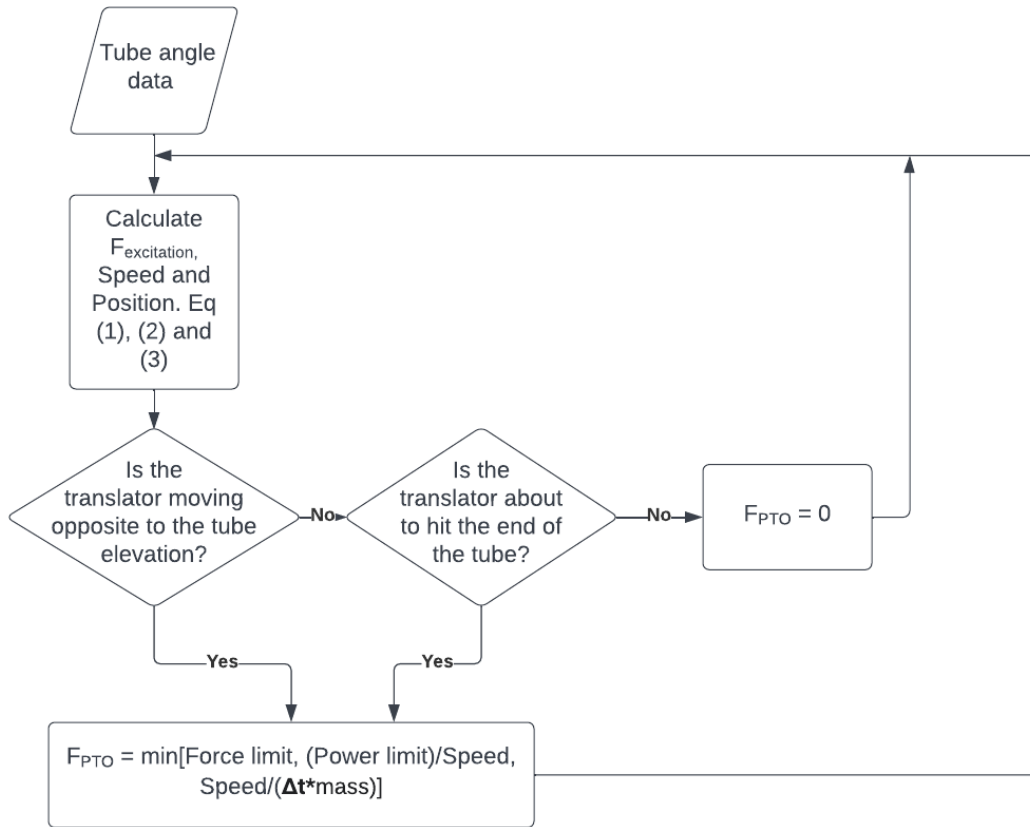
Figure 11: Binary PTO algorithm

2.4 Binary-Reactive PTO

Binary-reactive PTO is a combination of the binary damping and the reactive damping discussed earlier. This strategy applies a continuously varying reactive PTO force based on the position and speed of the sliding mass and when the binary damping conditions (PM translator hitting the end of the tube, or moving uphill) are met, the maximum power is extracted from the PM translator. Figure 12 shows the force profile of a binary-reactive PTO application. Figure 13 shows the corresponding position and speed values. It can be seen that the algorithm applies a force proportional to the position and

speed while the translator is near the center of the tube and applies the maximum force as the mass is about to hit the ends of the tube. It is interesting to observe that there is a step drop in force around the 617 s point. Here, the speed of the translator is high, therefore, an application of maximum force will lead to an instantaneous power that is greater than the power limit. Hence, the force is dropped to a lower magnitude. The power and force limits are discussed in Chapter The working of binary-reactive PTO algorithm is shown in Figure 14.
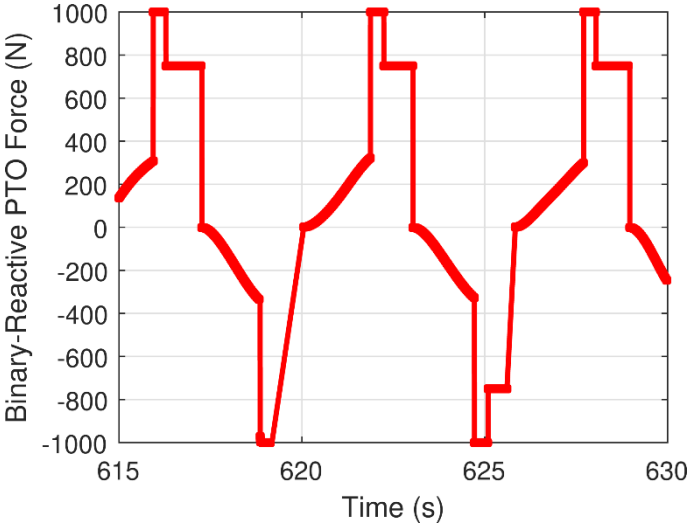
Figure 12: Binary-reactive PTO force profile
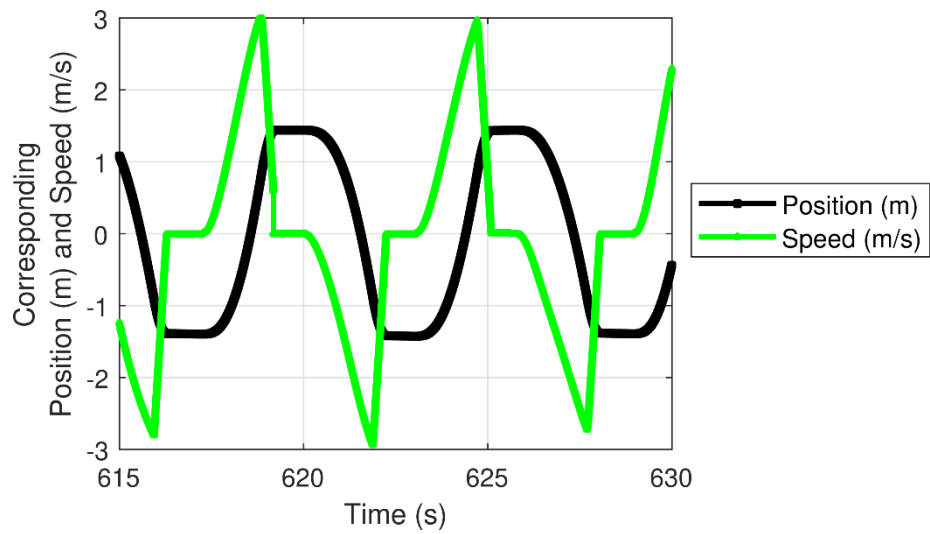
Figure 13: Binary-reactive PTO - Corresponding position and speed
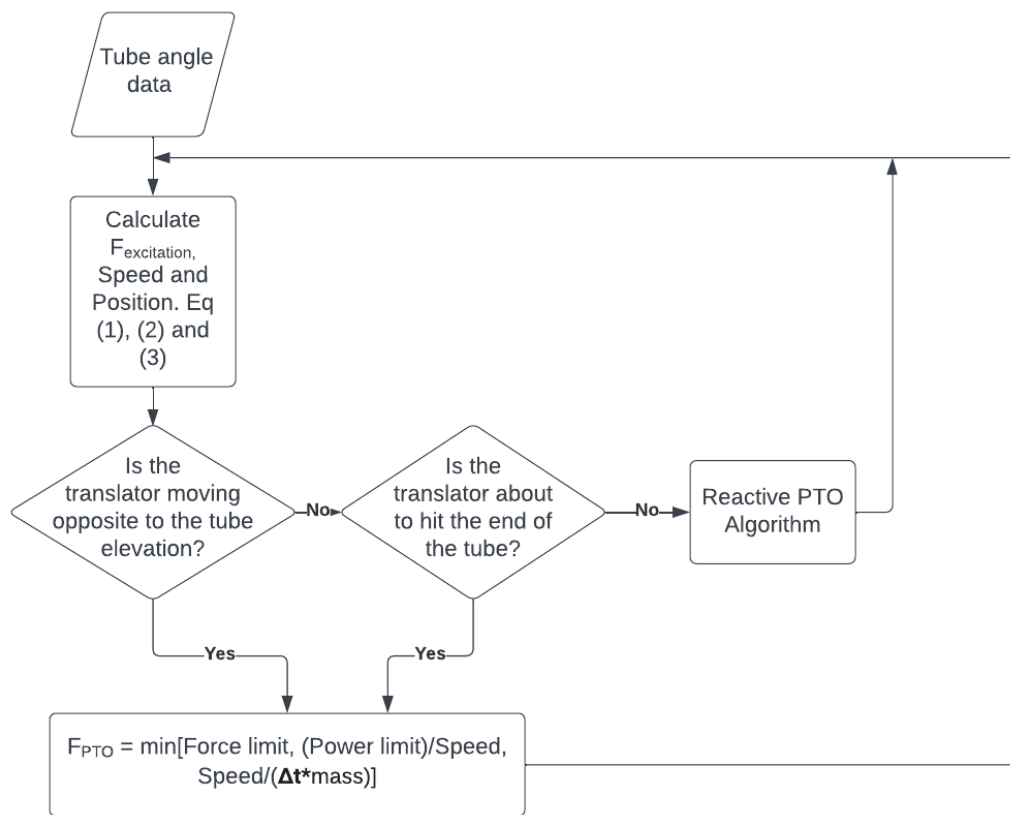
Figure 14: Binary-reactive PTO algorithm

16

2.5 Power and force limits

Two factors play an important role in the energy conversion process. The force limit of the linear generator determines the magnitude of energy capture and the power limit of the generator and associated power electronics determines how quickly this energy can be captured. It is required for a judicious selection of these two parameters as they directly affect the overall cost and size of the SR-WEC. If the limits are set too high, the capital expenditure of the system increases, while the returns in the form of increased average power may not be proportional. On the other hand, if the limits are set too low, it could result in sub-optimal capture of energy leading to a reduced energy capture. Therefore, the choice of power and force limits are non-trivial.

Since the binary damping involves the use of maximum force and energy capture in short periods of time, this PTO strategy was used to set the power and force limits of the study. From the hydrodynamic simulations, it was decided that for an optimal resonance with the ocean waves, the mass of the translator be 75 *kg* in mass and 0.3 *m* in length, with a total tube length of 3.18 *m.* This provides a total sliding length of 2.88 *m.* Further details of the generator dimensions are discussed in Chapter 4.

With these specifications, a parametric sweep of power and force limit was carried out for the binary PTO strategy. A set of 11 sea states were selected for this study. More details about this dataset is discussed in Chapter 3.
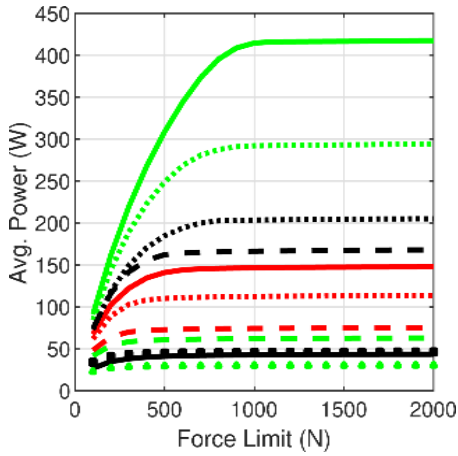
Figure 15: Parametric sweep of peak force limit. Reprinted with permission from [21]
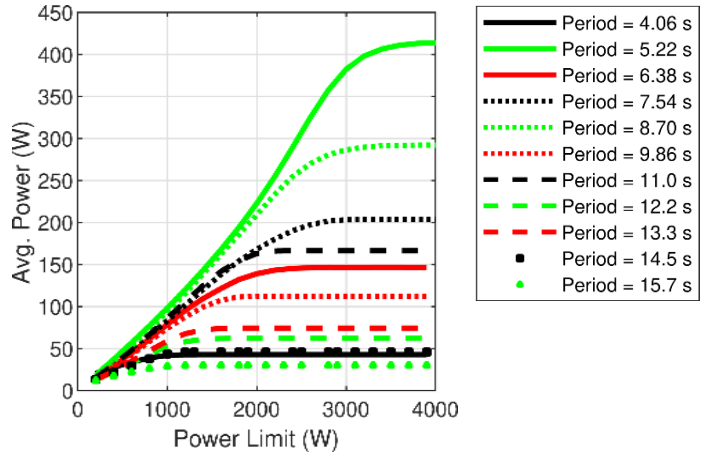
Figure 16: Parametric sweep of peak power limit. Reprinted with permission from [21]

Figure 15 shows the effect of increasing the force limit on the average power generated in the time series. It can be seen that increasing the force limit helps increase the average power to an extent. Beyond the optimal point, the increase in force limits has a diminishing return. Therefore, the optimal force limit is set to 1000 *N*. A similar trend is seen in Figure 16 with the effect of peak power limit on the average power generation. The optimal power limit is seen to be about 3000 *W*. These limits are used for the design of linear generator in Chapter 4.

2.6 Limitations in SR-WEC

The SR-WEC is a unique device that comes with its own set of challenges. As mentioned in the previous sections, the device is a tubular structure with a limited sliding distance. This makes it critical to ensure that the PM translator does not hit the ends of the tube while carrying a large kinetic energy. The choice of a higher force limit will provide enough headroom to apply large forces to prevent the damage to the walls of

18

SR-WEC. However, this increase in force limit comes at a cost. Therefore, a more suitable way to avoid damage to the tube is through an optimized PTO algorithm. The binary-reactive PTO is seen to be the best suited for this. It ensures that the kinetic energy is absorbed as the translator passes through the entire length of the tube, while applying a large enough force to stop it from hitting the ends of the tube with a high velocity.

3.   POWER TAKE OFF OPTIMIZATION AND COMPARISON[*]

For any PTO algorithm to work efficiently, it is important to optimize each algorithm to perform at its best. Once all the PTO algorithms are optimized, a fair comparison can be made for performance between the four PTO algorithms. It is important to optimize each PTO individually. This is because the optimal *Cpto* value for passive PTO may not be optimal for use in the reactive or binary-reactive PTO. The common parameters between the different strategies may not be optimal at the same value for all of them. In order to test the functioning of the PTO algorithms on a real world system, a dataset of random sea states consisting a time series of wave pitch angles is used.

3.1 Time series dataset of SR-WEC angle responses

A dataset of 11 random sea states with varying peak periods were used to compare the efficacy of the different PTO strategies. Wave spectral data is collected from National Data Buoy Center (NDBC) buoy #41002, located at a depth of 3920 m off the coast of Wilmington, North Carolina. The data consists of 7273 data points measured through 2018 [22]. The data is plotted as a resource characterization bin in Table 1 where each entry is the percentage of total data points that occurs in the given bin of significant wave height and energy period. The 11 peak periods, ranging from 4.06 s to 15.7 constitute 99.79% of all data points, representing a broad swathe of waves at the location. Using coupled time domain simulation of the SR-WEC, we obtained time series tilting motion data responding

---

[*] © 2021 IEEE. Part of this chapter is reprinted with permission from F. Naghavi, S. Sheshaprasad, M. Gardner, A. Meduri, H. Kang and H. Toliyat, "Permanent Magnet Linear Generator Design for Surface Riding Wave Energy Converters," in *Proc. IEEE Energy Convers. Congr. Expo.*, 2021, pp. 4369-4375

to respective random sea states and then solved the time domain sliding motions with the

different PTO loads coupled. The SR-WEC angle response for a portion of time is shown

in Figure 17.

Table 1: Resource Characteristic Bin of the Wave Data. Reprinted with permission from [21]

		Energy Period T_e(s)										
	Occurrence %	3.5	4.5	5.5	6.5	7.5	8.5	9.5	10.5	11.5	12.5	13.5
	0.25	0.00	0.00	0.07	0.18	0.23	0.00	0.00	0.00	0.00	0.00	0.00
	0.75	0.44	2.42	2.38	4.85	7.47	0.89	0.63	0.36	0.32	0.00	0.00
	1.25	0.61	5.57	8.11	3.88	8.84	1.28	1.10	0.30	0.36	0.00	0.01
	1.75	0.01	1.18	5.36	4.44	5.35	1.43	1.14	0.33	0.30	0.00	0.11
	2.25	0.00	0.15	2.13	3.69	2.43	0.39	0.67	0.15	0.23	0.10	0.01
	2.75	0.00	0.00	0.74	2.21	2.97	0.41	0.54	0.18	0.21	0.07	0.04
	3.25	0.00	0.00	0.10	1.27	2.43	0.44	0.23	0.11	0.06	0.12	0.06
	3.75	0.00	0.00	0.01	0.33	1.27	0.28	0.17	0.06	0.15	0.14	0.12
	4.25	0.00	0.00	0.00	0.04	0.61	0.36	0.25	0.03	0.10	0.11	0.12
Significant Wave Height H_s (m)	4.75	0.00	0.00	0.00	0.00	0.33	0.25	0.26	0.00	0.03	0.14	0.15
	5.25	0.00	0.00	0.00	0.00	0.06	0.12	0.17	0.03	0.06	0.12	0.12
	5.75	0.00	0.00	0.00	0.00	0.10	0.11	0.12	0.04	0.08	0.07	0.03
	6.25	0.00	0.00	0.00	0.00	0.03	0.04	0.11	0.04	0.03	0.06	0.21
	6.75	0.00	0.00	0.00	0.00	0.00	0.03	0.03	0.06	0.07	0.07	0.14
	7.25	0.00	0.00	0.00	0.00	0.00	0.00	0.01	0.00	0.08	0.03	0.08
	7.75	0.00	0.00	0.00	0.00	0.00	0.00	0.00	0.00	0.01	0.03	0.00
	8.25	0.00	0.00	0.00	0.00	0.00	0.00	0.00	0.00	0.01	0.00	0.01
	8.75	0.00	0.00	0.00	0.00	0.00	0.00	0.00	0.00	0.00	0.01	0.00
	9.25	0.00	0.00	0.00	0.00	0.00	0.00	0.00	0.00	0.00	0.00	0.00
	9.75	0.00	0.00	0.00	0.00	0.00	0.00	0.00	0.00	0.00	0.00	0.00
Peak Period T_p(s)		4.06	5.22	6.38	7.54	8.7	9.86	11.02	12.18	13.34	14.5	15.66
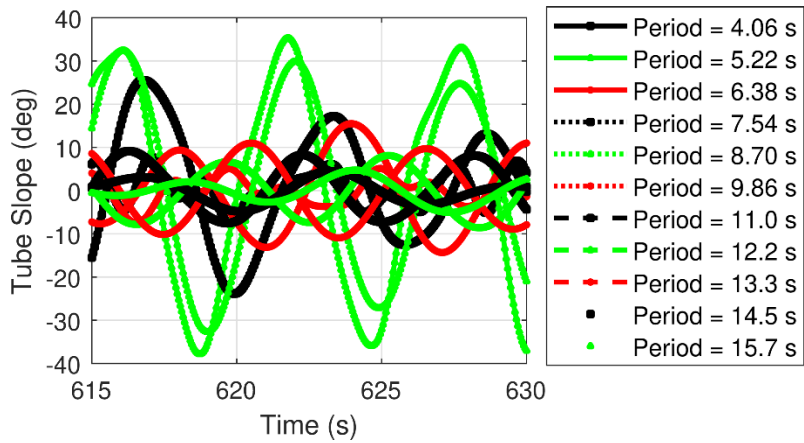
Figure 17: SR-WEC angle response

3.2 PTO tuning and optimization

Since the dataset comprises of irregularly excited waves, the impedance matching equations do not provide the optimal damping coefficient values. Therefore, the viscous damping and stiffness coefficients are determined by running an extensive parametric sweep of the variables for each time period and choosing the values that provided the maximum average output power for the majority of the wave spectrum. A ballpark starting point for K_{PTO} is chosen using the impedance matching equation (6) and then sweeping the variable around this point. While optimizing the reactive for random waves, the $peakPeriod$ is set by performing a spectrum analysis of the waves and determining the dominant period in the time series. The C_{PTO} coefficient is parametrically varied within a set range. The optimization flow for passive PTO is shown in Figure 18. Similarly, the optimization flow of reactive PTO is shown in Figure 19.

The binary PTO is optimized by including a binary timing term termed as *binary factor* that determines how early or late the PTO force is turned ON. This number is a fraction of the tube length and it is parametrically varied to find the best value providing the maximum average output power. The binary PTO optimization workflow is shown in Figure 20. Binary-reactive PTO optimization involves a combination of both reactive and binary parts of the system. The C_{PTO} and K_{PTO} coefficients are optimized according to Figure 19 and then the binary factor term is optimized according to Figure 20.
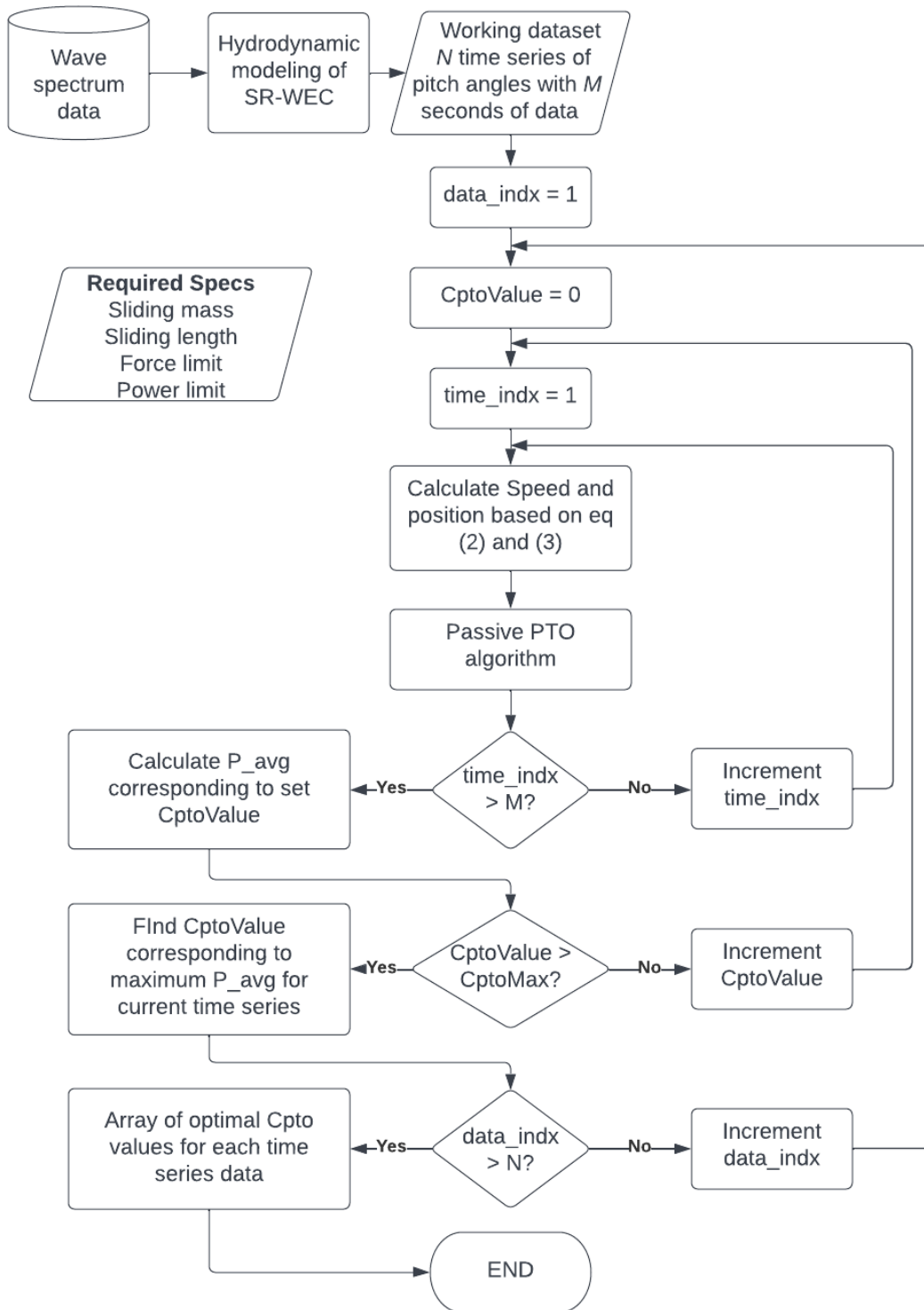
Figure 18: Passive PTO optimization flow
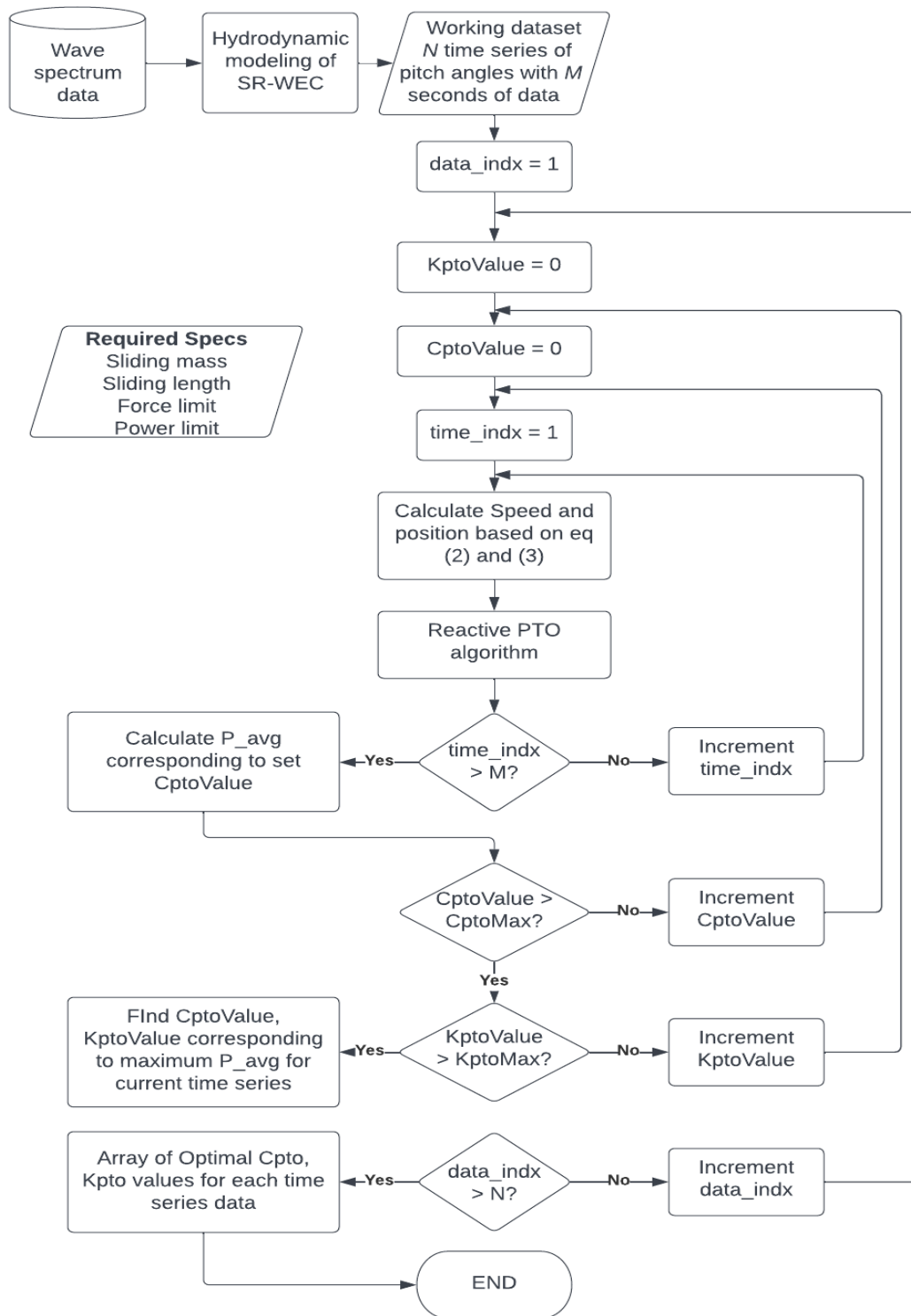
Figure 19: Reactive PTO optimization flow
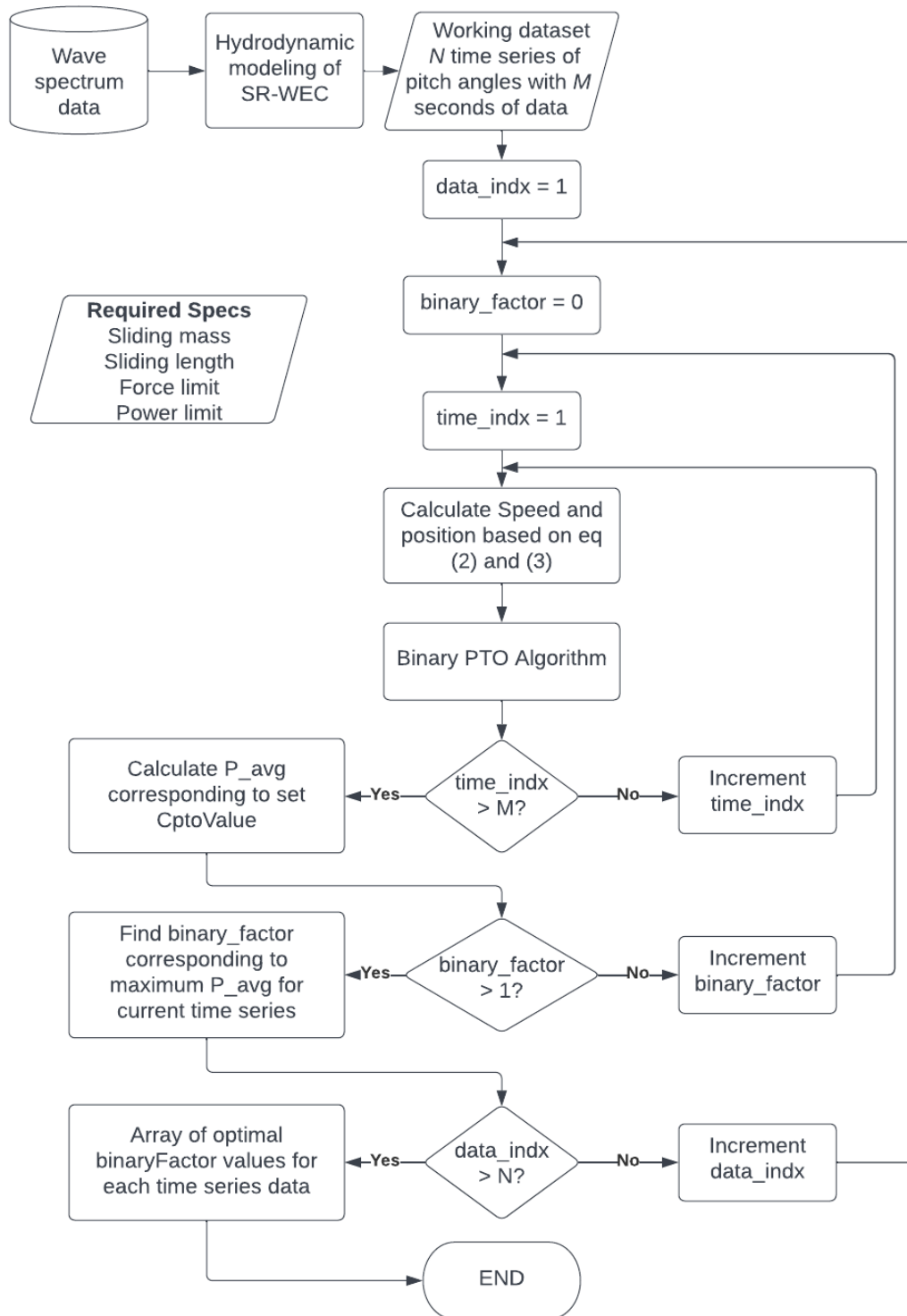
Figure 20: Binary PTO optimization flow

3.3 Results

The four PTO strategies were optimized for the given dataset. Since the dataset is representative of the real-world conditions that will be encountered by the SR-WEC in the sea, it can be used to represent the power generation capability of the SR-WEC at that location for the lifetime of its operation. These numbers do not account for the efficiencies of the linear generator or the controlled rectifier, as that is a variable controlled by the optimal design of the machine and power electronics. The averaging for the power is done only on the second half of the dataset as the first half includes the ramping up of the hydrodynamic simulation, which is a transient state. The average power outputs of each sea state for each PTO strategy is tabulated in Table 2.

Table 2: Average output powers for different PTO strategies

Peak period (s)	Average output power (W)			
	Passive PTO	Reactive PTO	Binary PTO	Binary Reactive PTO
4.06	17.67	36.25	42.38	85.22
5.22	330.47	334.79	355.75	364.68
6.38	86.59	100.33	134.82	128.28
7.54	131.3	141.39	185.31	167.85
8.70	204.56	212.51	261.15	244.39
9.86	62.33	79.44	104.86	107.94
11.0	100.44	116.33	152.78	147.57
12.2	30.21	46.94	58.8	67.66
13.3	37.56	55.8	70.11	78.75
14.5	19.91	39.07	44.14	58.62
15.7	13.26	28.1	29.37	44.59

From the table above, it can be seen that passive PTO produces the least average power across all sea states. This is in line with the literature that passive damping is sub-optimal for energy capture from both regular and random waves. Reactive PTO produces significantly better average power output for a majority of the sea states and smaller gains are seen in other sea states. This bolsters the argument that output power is improved when using reactive PTO over passive PTO strategy. As the wave slopes are not sinusoidal, passive PTO is not the most optimal strategy as impedance matching is not possible in every instant. Therefore, a more discrete strategy is more suitable. This can be seen by the increase in output power for the binary PTO. There is again a significant improvement in average output power compared to reactive PTO. When a combination of reactive and binary algorithms is used in the form of binary-reactive PTO, the power output is seen to be better in the sea states with peak periods 4.06 s, 5.22 s, 9.86 s, 12.2 s, 13.3s, 14.5 s, and 15.7 s. While, the binary PTO performs better in the 6.38 s, 7.54 s, 8.7 s, and 11.0 s sea states. Considering the probability of occurrence of each sea state (from Table 1), the average output of binary-reactive PTO is about 4.5% improvement over the binary PTO. Table 3 shows the percentage difference in the weighted average output power between the different PTOs. Weighted average is calculated by multiplying the average power in each state with its corresponding percentage of occurrence.

28

Table 3: Percentage difference between PTO strategies

Percentage Variation (%)	Passive PTO	Reactive PTO	Binary PTO	Binary-Reactive PTO
Passive PTO	N/A	19.89	46.57	53.23
Reactive PTO	-16.59	N/A	22.26	27.81
Binary PTO	-31.78	-18.21	N/A	4.54
Binary-Reactive PTO	-34.74	-21.76	-4.34	N/A

4.   LINEAR GENERATOR DESIGN[*]

The PM Tubular Linear (PMTL) generator has been recognized as a suitable candidate for wave energy converters [23-30]. A PM generator offers a higher force density and higher efficiency than other types of generators [24]. Various tubular PM generators have been proposed with radial, axial, and Halbach array magnet arrangements [23, 25, 27-30]. One challenge for tubular PM generators is the cogging force due to the stator teeth [23, 30], which can reduce the amount of power the SR-WEC is able to extract from the waves, especially in sea-states with small waves. To eliminate the cogging force, a slotless stator design has been adopted for the generator designed in this study. In addition, to avoid cable stress and reliability issues due to movement, the stator windings are placed on the stationary part of the generator as shown in Figure 21. The length of the stator and, thus, the generator can be modularly increased according to the required length from power take-off (PTO) studies. However, only the overlapping region between the translator (magnets) and the stator winding produces generation force at any instant.
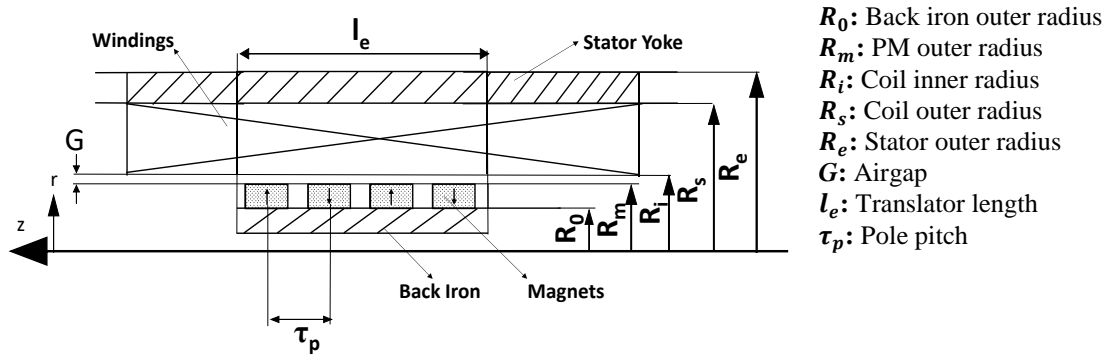
Figure 21: PMTL Generator Geometry. Reprinted with permission from [21]

4.1 Generator design approach and parameters

Figure 21 shows the architecture of the generator. It consists of back iron, radially magnetized magnets, and outer windings on the stator. A similar design is proposed in [28, 29] where an analytical solution has been represented for the design of such generators. However, in this study, the design analysis is done using parametric finite element analysis (FEA) simulations of the generator in ANSYS Maxwell. Due to the simplicity of the design and its symmetry around the axis, parametric 2D simulations are used to rapidly characterize its performance. The design parameters and the acceptable range for each one is listed in Table 4. Based on these ranges, all the cases are generated and simulated. There are two constraints for the design of the generator: 1) The minimum acceptable outer radius for the shaft is set to 50 *mm* so it can withstand the translator weight without significant deflection 2) The total outer radius of the generator (R_e) should be less than 105 *mm* to fit inside the SR-WEC. Therefore, the cases that do not satisfy these two constraints are not considered. A total of 8160 cases were simulated for this study.

31

Table 4: PMTL generator parameters. Reprinted with permission from [21]

Design Parameter	Range
Shaft Radius	50 mm
Magnet thickness ($T_m = R_m - R_0$)	2-10 mm
Back iron thickness	5-25 mm
Translator length (l_e)	100-300 mm
Translator poles	2-12
Winding thickness ($R_s - R_i$)	10-30 mm
Airgap (G)	1mm
Stator Yoke	5 mm
Copper Fill Factor	75%

4.2 Optimization of the generator design

Based on the PTO study, the generator requires a force rating of 1000 *N* and a power rating of 3000 *W*. Parametric magnetostatic simulations are used to characterize the impacts of the design parameters, and transient simulations are performed to check the back-emf and force ripple of the best designs. The airgap is assumed to be 1 *mm*, and a rms current density of 5 A/mm^2 at peak force is assumed for the windings.

Figure 22 show the effect of the winding thickness for different values of magnet thicknesses, which indicates the effects of magnetic loading and electric loading on the generator force. The results shown in Figure 22 are the highest translator force for each magnet thickness and winding thickness while letting the translator length, pole count and back iron thickness vary freely over the range of values mentioned in Table 4. As seen in Figure 22, the force plateaued after a certain winding thickness due to the reduced flux density in the outer turns. Additionally, as the thickness of PM and winding is increased,

32

the back-iron thickness reduces to meet the 105 mm outer radius constraint, which reduces

the force for the highest winding and magnet thicknesses. However, generally, the increase

in magnet thickness increases the force for various values of coil thickness because

increasing the magnet thickness increases the flux density, as well as increasing the air gap

radius. In order to minimize the cost, a magnet thickness of 4 mm and a winding thickness

of 5 mm are selected.
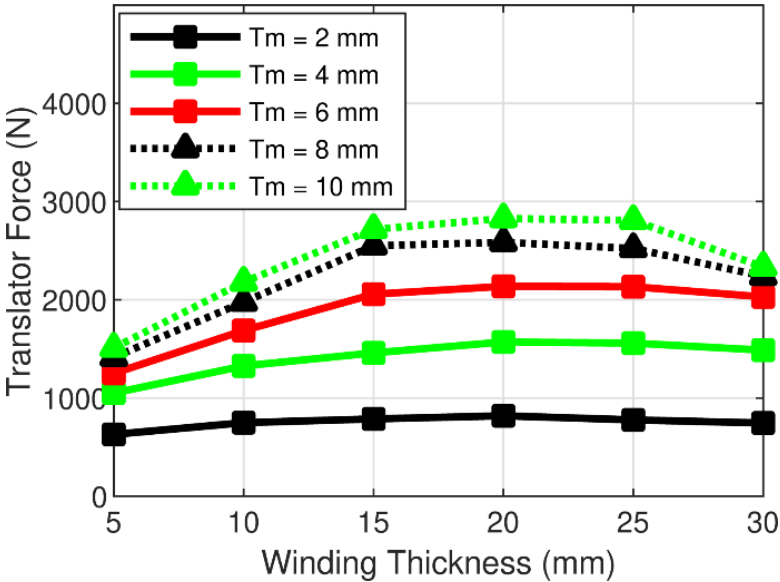
Figure 22: Force vs winding thickness for different magnet thicknesses. Reprinted with permission from [21]

Figure 23 shows the effect of the translator length for pole counts with magnet and

winding thicknesses of 4 *mm* and 5 *mm* respectively. The minimum and maximum

allowable lengths for the translator are 100 *mm* and 300 *mm*, respectively. The pole pitch,

number of poles and translator length need to be determined. Referring to Figure 23, a

translator length of 300 *mm* with 8 poles satisfies the 1 *kN* force requirement.

Next, the thickness of the back iron is selected. According to Figure 24, increasing the back-iron thickness increases the force. With the given constrains, a back-iron thickness of 25 *mm* is chosen. The thickness of the stator yoke does not significantly affect the force production. However, removing the stator yoke completely does result in a force reduction of about 14%. Consequently, the back iron and stator thickness of 25 *mm* and 5 *mm* are selected, respectively.
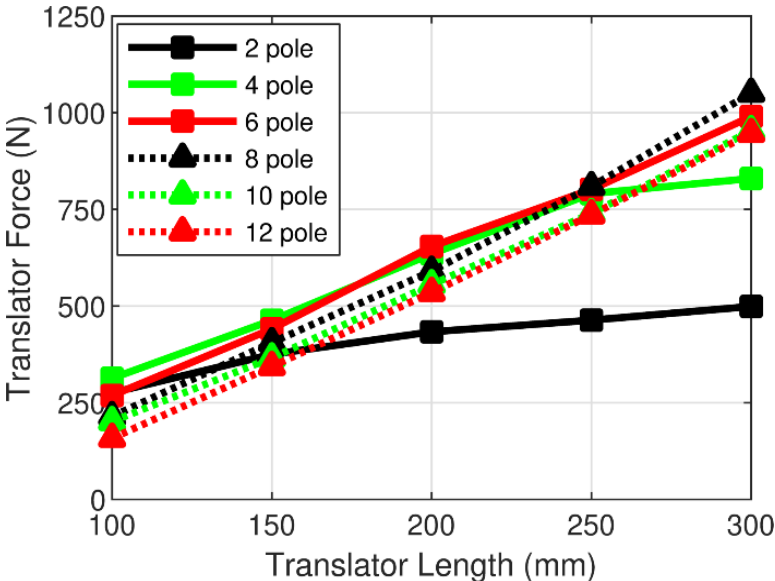
Figure 23: Force vs translator back iron thickness for different stator yoke thickness. Reprinted with permission from [21]
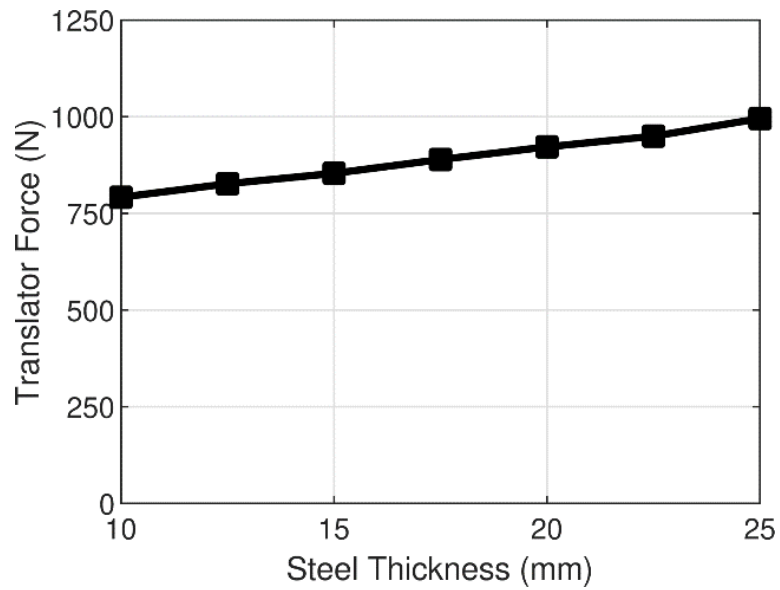
Figure 24: Force vs translator back iron thickness. Reprinted with permission from [21]

4.3 Winding design

The number of turns for each winding is determined to produce the Ampere-turns according to the designed winding area. As shown in Figure 25, there is one coil per phase per pole. With a current density of 5 A/mm^2, winding thickness of 5 *mm* and pole pitch of 37.5 *mm*, each coil is designed to have 90 turns of 20 AWG wire. The force ripple predicted by transient simulation is less than 4% of the average force which is acceptable for this application. The final specifications of the generator are summarized in Table 5.
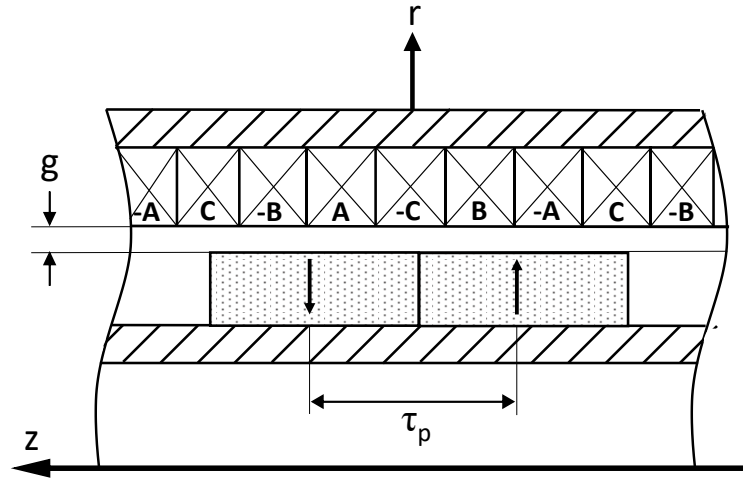
Figure 25: Winding design. Reprinted with permission from [21]

Table 5: PMTL generator specifications. Reprinted with permission from [21]

Design Parameter	Value
R_0	75 mm
R_m	79 mm
R_i	80 mm
R_s	85 mm
R_e	90 mm
l_e	300 mm
Translator poles	8
G	1 mm
τ_p	37.5 mm
Translator Back Iron	25 mm
Stator Yoke	5 mm
Turns per Coil	90
Magnet Type	N50

4.4 Experimental prototype

A smaller prototype with similar architecture is designed and fabricated to investigate the performance of the PMTL generator inside the SR-WEC. The prototype

36

is cautiously designed and serves as a proof of concept prototype. Table 6 lists the

parameters and dimensions of the prototype.
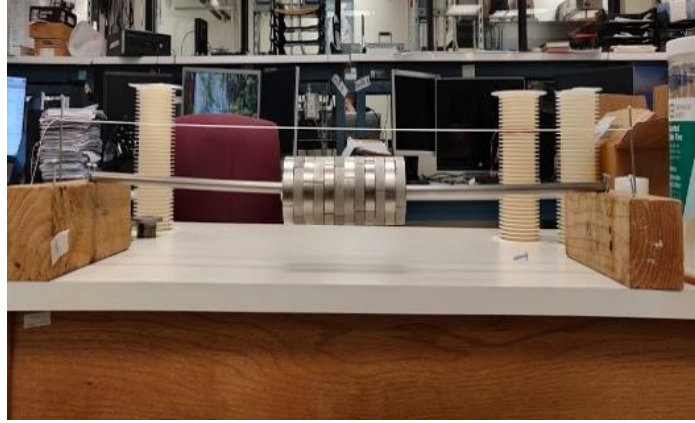
Figure 26: PM translator of the prototype. Reprinted with permission from [21]

The translator is assembled using commercially available N42 magnets with a total of 12

poles. The back iron inner radius is 6 mm and its outer radius is 31.75 *mm*. The pole pitch

is 19.05 *mm*. The magnet thickness is 6.35 *mm* and each pole consist of 4 arc magnets.

Figure 26 shows the PM translator.

Table 6: Specifications of the small PMTL prototype. Reprinted with permission from [21]

Design Parameter	Value
R_0	31.75 mm
R_m	38.1 mm
R_i	41.1 mm
R_e	51.1 mm
l_e	228.6 mm
Translator Poles	12
G	3 mm
ς_p	19.05 mm
Translator Back Iron	23.25 mm
Turns per Coil	70
Magnet Type	N42

The stator is fabricated using additive manufacturing. The total stator length is 914.4 *mm*, so the translator can travel a maximum distance of 685.8 *mm* inside the stator. Each coil has of 70 turns of 20 AWG wires all connected in series. FEA simulations show that the prototype is capable of producing 140 *N* at its rated peak current of 3.66 *A*. A testbed was built to emulate the wave motion, as shown in Figure 27. It includes two stepper motors, ball screws, and springs. By controlling the motors according to wave frequency and amplitude, the prototype can be tilted with different frequencies and slopes to evaluate the generator for different emulated sea states.
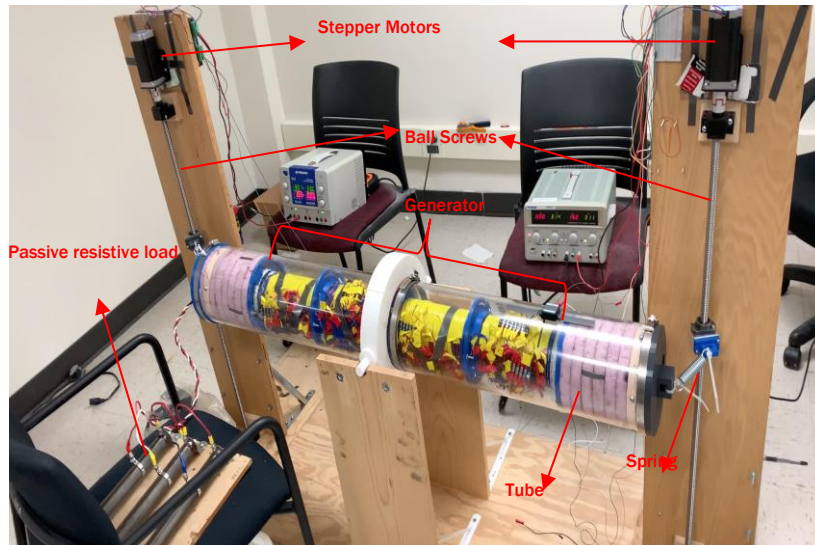
Figure 27: Assembled prototype and testbed. Reprinted with permission from [21]

The 22 stator windings can be connected in series or parallel. Series connection results in high resistance and low efficiency. However, parallel connection can result in circulating currents. In the initial stages, the generator is tested with series connection of windings due to its simplicity. Measurements with LCR meter show an inductance of 44 *mH* and resistance of 67.2 Ω measured line-line with the series connection.

In the initial stages, only a resistive three-phase load was used. The generator terminals are connected to a three-phase resistive load with 33.6 Ω in each phase. Therefore, over 50% of the generated power by the generator is dissipated in the windings due to series connection of the windings.

Figure 28, shows phase voltage, current, and instantaneous three-phase output power for a sliding angle of 40°. The phase current and terminal voltage peak at 18.8 *V* and 0.57 *A*, respectively. At 40°, the total three-phase instantaneous power goes up to 16 *W* immediately before the translator reaches the end of the stator around 1.1 *s*.

Figure 29, shows the generator phase voltage, current, and instantaneous three-phase output power for a sliding angle of 50°. At this angle, the translator speed is higher when it reaches the end of the stator around 0.95 *s*, so the peak current, voltage and power are higher as well. The peak voltage and current are 23.69 *V* and 0.75 *A*, respectively. The three-phase instantaneous power goes up to about 28 *W*.

As stated previously, 50% of the generator power is dissipated in the stator windings due to the large resistance of the series connection and the selection of the load resistance.
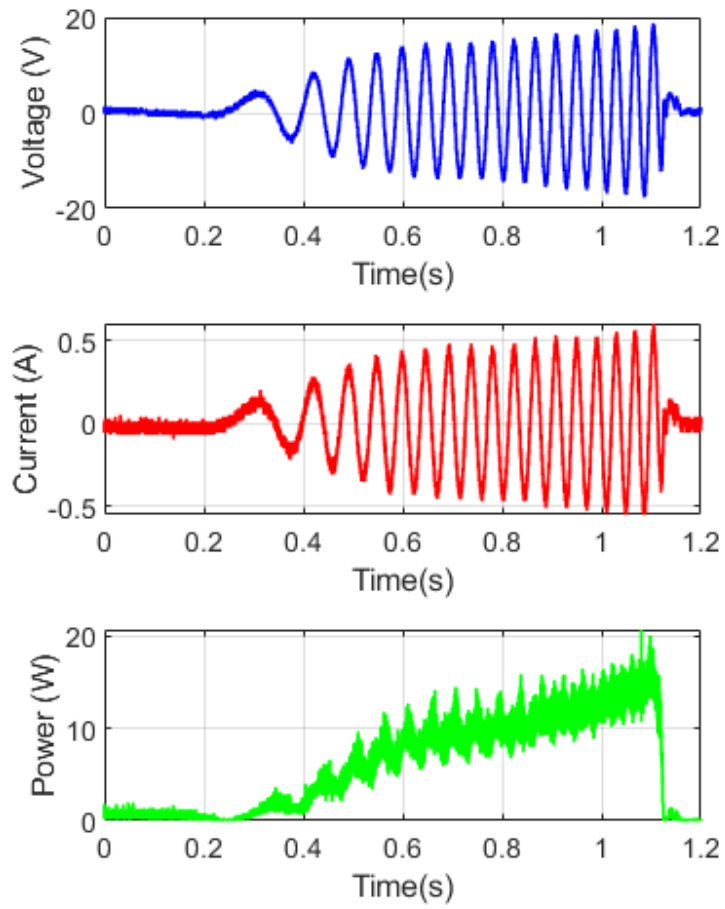
Figure 28: Generator line-to-neutral voltage, current and three phase power output at 40° sliding angle. Reprinted with permission from [21]
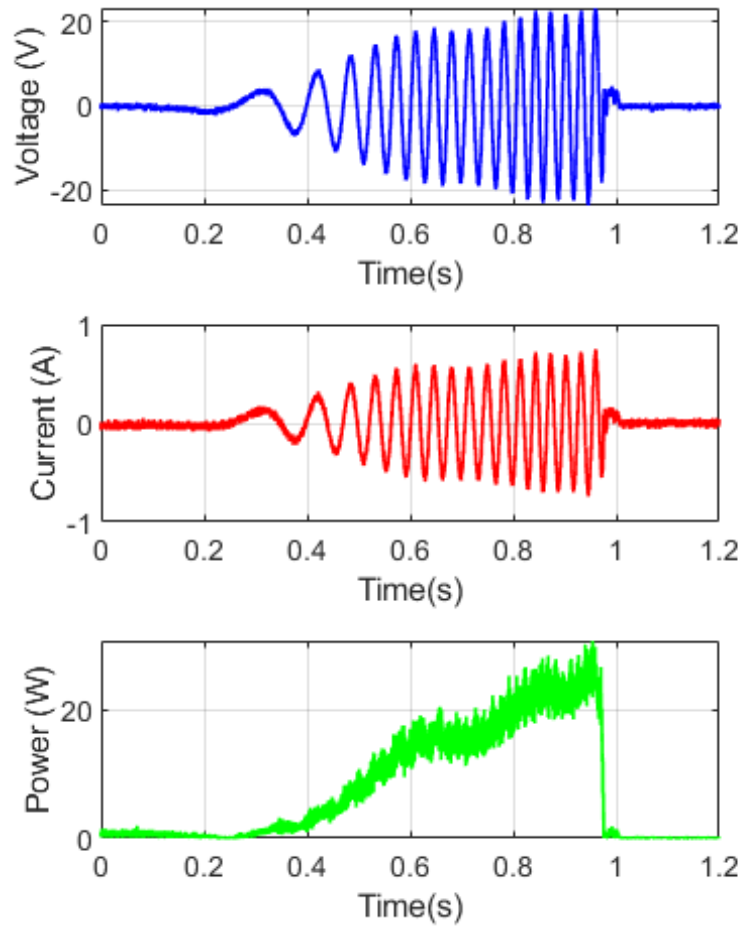
Figure 29: Generator line-to-neutral voltage, current and three phase power output at 50° sliding angle. Reprinted with permission from [21]

4.5 Challenges in prototyping

There were several challenges in building and testing the small-scale prototype. The air gap was uneven as the center rod holding the PM translator was bending under the weight of the magnet assembly. 3-D printed stators failed at the ends of the SR-WEC as the translator was hitting the ends of the tube with significant velocity. Actuators on the testbed failed as the support structure was not strong enough. These challenges prevented

41

the PTO testing on the small-scale prototype. Hence, a commercially available set of machines were used for the PTO testing. This will be discussed in the next section.

5.   EXPERIMENTAL TESTING

In the previous chapters we discussed about the four types of PTO algorithms, their optimization and simulation results. Then we discussed about the linear generator design and the challenges associated with the small-scale prototype. In this chapter, we will discuss the experimental implementation and verification of the PTO control strategy. In order to test the PTO algorithms, we need one linear machine acting as a generator and another machine that can act as a prime mover.

5.1 Experiment setup

For this test, an existing testbed consisting of an AC servo motor (Allen Bradley 1326AB) coupled with a trans-rotary magnetic gear (TROMAG) was chosen. The TROMAG is a magnetic gear that converts a high speed low torque input to a high force low speed output and vice-versa [31]. This arrangement is coupled to a linear machine (LinMot PS10-70x400U-BL-QJ) with a 1.1 m long translator and a 0.5 m stator. This is used as a linear generator. Both the machines are rated to operate with a three phase supply of 480V AC. The AC servo motor is rated for a peak torque of 13 $N.m$ with a rated speed of 3000 RPM. While the linear motor is rated for a peak force of 2.7 kN with a rated velocity of 3.9 m/s. The testbed setup is shown in Figure 30. Texas Instruments TI TMDSHVMTRPFCKIT high voltage motor control and PFC kit, paired with a piccolo TMS320F28035 control card, is used to control the linear machine. And an educational development motor control kit, paired with a delfino TMS320F28335 control card, is used to control the AC servo motor. The inverter and controlled rectifier setup is shown in Figure 31. A sensorless field oriented control (FoC) is used to control the linear machine.

While a sensored FoC with linear encoder is used to control the AC servo motor coupled with the TROMAG. Although the inverters had a peak DC bus voltage of 350 V, a DC power supply with a maximum supply voltage of 150 VDC was used to maintain safe operating conditions in the laboratory. The three phase inverters have a peak current limit of 2.3 *A* without external cooling. Hence, the maximum current from the DC supply was limited to 2 *A*.

Figure 30: Testbed setup

The gear ratio of the TROMAG is given by:

$$G = \frac{\omega}{v} = \frac{2\pi}{P\tau_p} = \frac{F_t}{T_r} \tag{5}$$

where, τ_p is the pole pitch of the TROMAG, P is the number of poles. ω is the rotary speed, v is the linear speed, F_t is the translating force, and T_r is the rotary torque. For the given machine, the gear ratio is $G = 309.2 \; m^{-1}$. Therefore, to run the linear machine at speed of 1 *m/s*, the rotary machine needs to rotate at 309 rad/s (~2950 RPM).
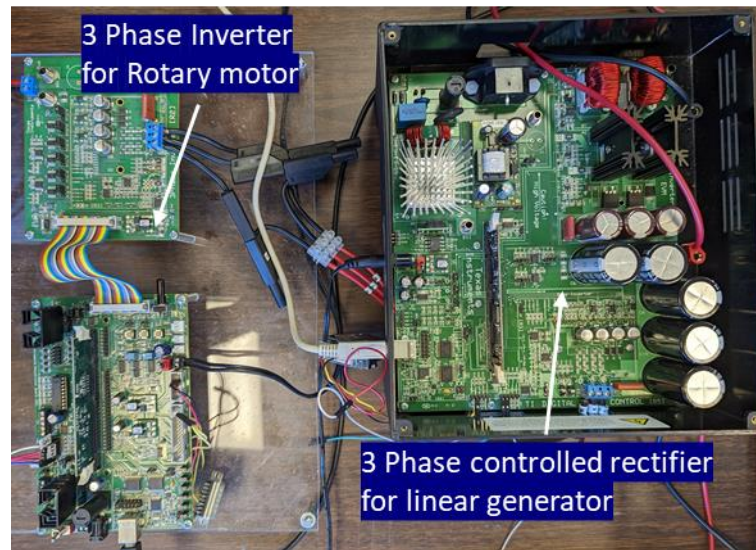
Figure 31: Inverter and controlled rectifier

5.2 PTO results

In the experimental setup, the DC bus voltage is limited to a 150V DC. Hence, the maximum rotary speed achievable was 450 RPM, which results in a maximum linear speed of 0.152 *m/s.* For the PTO testing, field oriented speed control was used to control the prime mover's rotary speed. The speed was commanded in a sinusoidal fashion with the peak speed reaching 450 RPM. The sinusoidal function had a period of 6 s. Due to the friction present in the system, the speed control was not effective and the motion was not a pure sinusoid. Since the PTO testing required the use of a random wave with a fundamental sinusoid, this excitation motion was representative of a random sea state.

With the prime mover moving the linear translator in a random fashion, sensorless field oriented current control is used to apply force in line with the passive and reactive PTO algorithms.

5.2.1 Passive PTO results

The passive PTO algorithm is applied on the linear generator. Here, the force is directly proportional to the speed of the translator. The algorithm was run at three different values of the viscous coefficient, C_{PTO}. The average powers of the three tests are reported in Table 7. It can be seen that the case with $C_{PTO} = 0.2$ is the optimal case for this PTO. The DC voltage, current and power waveforms for the case with $C_{PTO} = 0.2$ is shown in Figure 32.

Table 7: Average powers for passive PTO

C_{PTO}	Avg. Power (W)
0.2	0.884
0.5	0.715
2.0	0.805
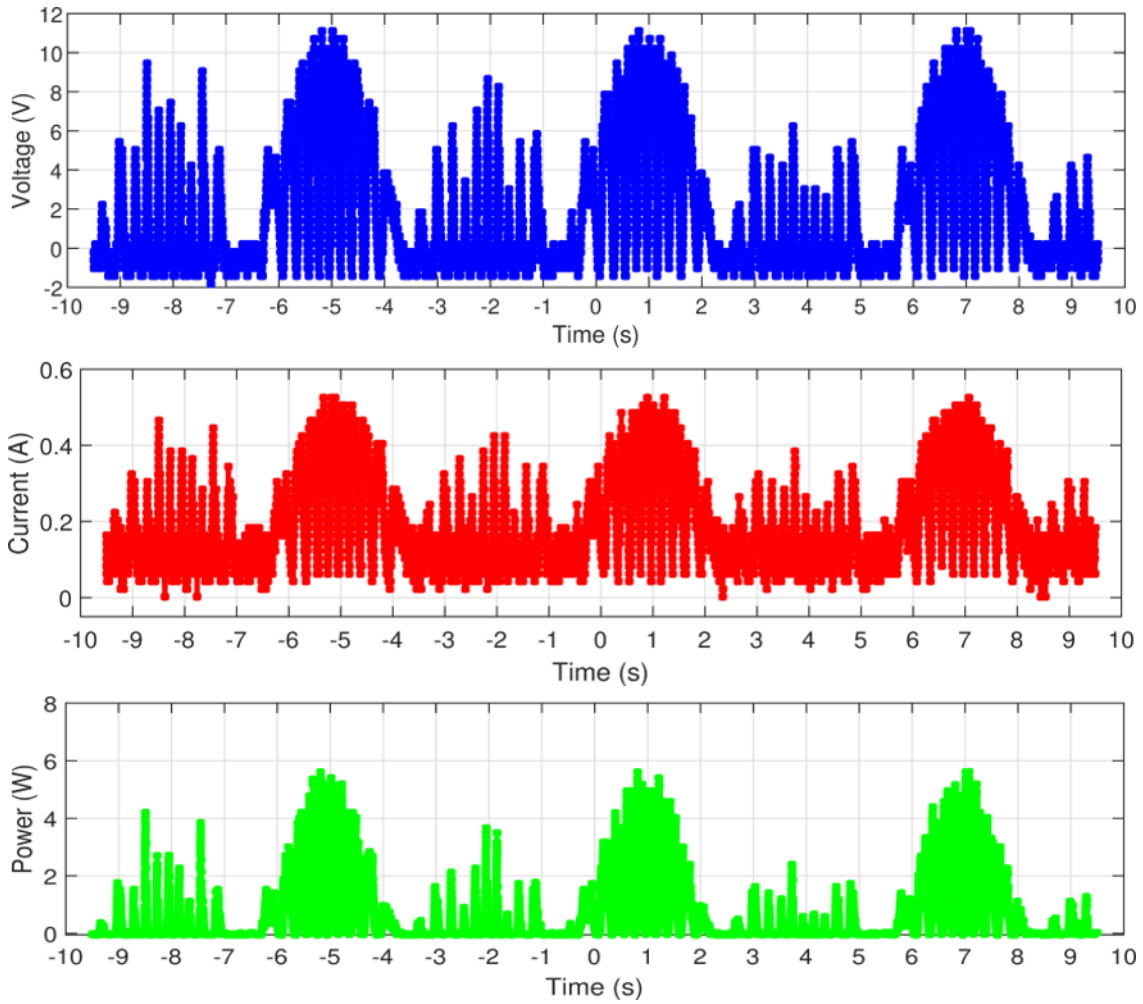
Figure 32: Passive PTO - DC voltage, current and power

5.2.2 Reactive PTO results

The reactive PTO algorithm is applied on the linear generator by setting the force as a function of speed and position of the PM translator. The algorithm was run at six different combinations of the viscous and the stiffness coefficients. The average powers of the six tests are reported in Table 8. It can be seen that the case with $C_{PTO} = 0.5$ and $K_{PTO} = 0.9$ is the optimal case for this PTO. The DC voltage, current and power waveforms for this is shown in Figure 33.

47

Table 8: Average powers for reactive PTO

C_{PTO}	K_{PTO}	Avg. Power (W)
0.2	0.9	0.777
0.2	2.0	0.824
0.5	0.9	1.164
0.5	2.0	0.702
2.0	0.9	0.692
2.0	2.0	0.722
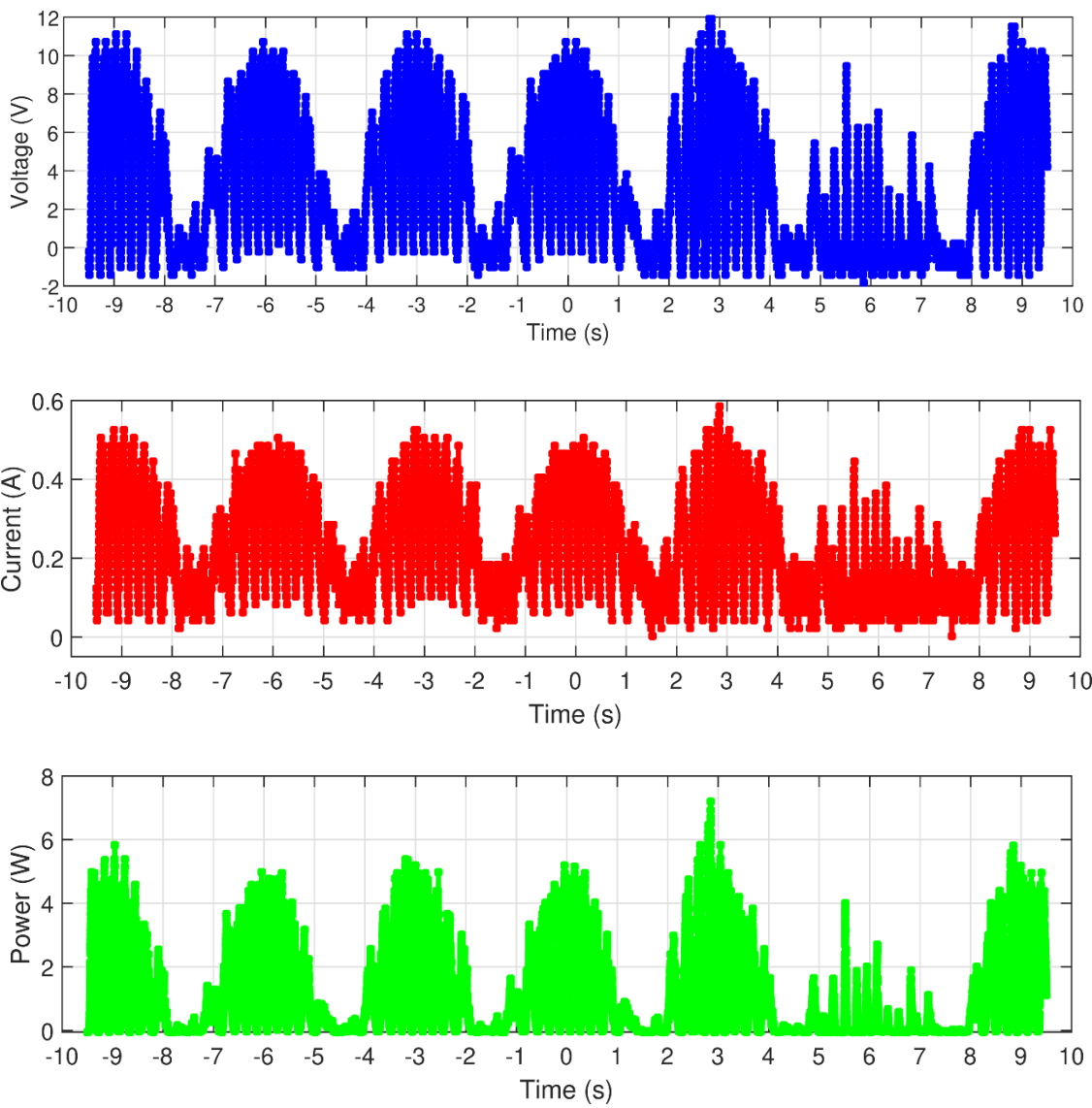
Figure 33: Reactive PTO - DC voltage, current and power

48

5.3 Challenges with experimental setup

The testbed setup worked well for demonstrating the difference between the performance of the passive and reactive PTO strategies. However, there were some challenges in this setup which prevented the ideal testing of PTO strategies. The linear machine has very poor efficiency at low speeds. The linear machine does not have any bearings. The PM translator slides on a plastic sleeve inside the stator. This results in large static friction when moving the translator. The friction in the linear machine gets geared back into the prime mover through the TROMAG. This makes it extremely difficult to apply stepped forces that is required by the binary PTO strategy. Applying a step load through the TROMAG results in a very large torque developed on the motor. Since the supply is limited to $2\,A$, the motor cannot provide the necessary torque. Thus, testing of the binary PTO was not possible on this setup. The objective of this experimental study was to show that PTO control algorithm can be implemented on a linear machine. This objective has been met.

6.   CONCLUSION

This study has introduced the different types of WECs. Namely oscillating water column, overtopping devices and oscillating body type WECs. The focus was then put on the newly invented surface riding wave energy converter. A brief introduction of the SR-WEC has been provided. The SR-WEC has the advantage of being able to produce electricity at a competitive LCOE, while maintaining a long operating life without requiring regular maintenance. This makes it ideal for small and medium scale wave energy generation. The

The power take-off strategies were examined. The traditional PTO methods of passive and reactive were studies, and the novel binary and binary-reactive PTOs were introduced. The functioning of these algorithms was provided in detail in Chapter 2. The selection of power and force limits were shown comprehensively. The limitations of PTO with respect to SR-WEC were also discussed.

The dataset used for the PTO optimization was introduced. It was shown that a selection of 11 sea states covered roughly 94% of all the sea state occurrences. The PTO tuning and optimization workflow was explained in detail. Tuning was done on the dataset containing the 11 sea states mentioned above. The optimization of passive PTO involved the selection of optimal C_{PTO} for each sea state's time series. The reactive PTO optimization included the optimal selection of the C_{PTO} and K_{PTO}. The binary PTO optimization involved the tuning of the *binary factor* which controlled the delay with which the generator turns on when the translator is at the end of the tube. The binary-

reactive PTO tuning involved the selection of all three factors, i.e. C_{PTO}, K_{PTO}, and the *binary factor*.

Once the PTOs were optimized, the average output powers for each PTO at each sea state was computed. This showed that the passive PTO is the least optimal for use in the SR-WEC, followed by the reactive PTO, then the binary PTO and the most optimal PTO for the SR-WEC was shown to be the binary-reactive combination providing about 53% improvement in weighted average power compared to the passive PTO.

A slotless permanent magnet tubular linear generator was proposed for use in the SR-WEC. The design and optimization of this 1 kN, 3 kW PMTL generator was discussed. The effect of winding thickness, magnet thickness, pole count, translator length, and back iron thickness on the generator force was discussed. It was shown that in order to meet the force requirements, either the thicker winding sections could be used, or thicker magnets can be used. A balance was struck between these two parameters keeping the cost in mind. Similarly, the translator length and pole counts were chosen such that the force target could be achieved at the minimal cost. The analysis was carried out by running a total of 8160 2D static simulations on ANSYS Maxwell. The simulations also set maximum and minimum ranges for the puter radius of the shaft, output radius of the generator and maximum length of the PMTL generator so that it fits well into the SR-WEC cylinder. A small scale prototype was built for testing and validating the design of the linear generator. The challenges associated with this are also detailed.

Finally, an experimental setup to test the PTO controls was introduced. This

setup consists of a rotary motor coupled with a trans rotary magnetic gear. The

TROMAG converters the high speed low torque rotary motion into low speed high force

translating motion. The TROMAG is mechanically coupled to the PM translator of a

linear generator. An inverter is used to control the speed on the rotary motor, while a

controlled rectifier is used to control the force applied by the linear generator. The

passive and reactive PTO algorithms were tested on this setup. It was shown that the

reactive PTO performs better than the passive PTO, which is in line with the literature

and simulation results. Since the liner motor and TROMAG are not made for an

instantaneous application of large force, the binary and binary-reactive PTOs could not

be tested. However, the objective of the test was met since it was shown that the PTO

control algorithms can be implemented on linear machines.

REFERENCES

[1]   S. Barstow, G. Mørk, D. Mollison, and J. Cruz, "The Wave Energy Resource," in
        Ocean Wave Energy: Current Status and Future Prespectives, J. Cruz Ed. Berlin,
        Heidelberg: Springer Berlin Heidelberg, 2008, pp. 93-132.

[2]   R. Bedard *et al.*, "North American ocean energy status-March 2007," *Electric
        Power Research Institute (EPRI) Tidal Power (TP),* vol. 8, p. 17, 2007.

[3]   A. Clément *et al.*, "Wave energy in Europe: current status and perspectives,"
        Renewable and sustainable energy reviews, vol. 6, no. 5, pp. 405-431, 2002.

[4]   D. Magagna and A. Uihlein, "Ocean energy development in Europe: Current
        status and future perspectives," *International Journal of Marine Energy,* vol. 11,
        pp. 84-104, 2015.

[5]   J. Falnes, "A review of wave-energy extraction," *Marine structures,* vol. 20, no.
        4, pp. 185-201, 2007.

[6]   S. Prakash *et al.*, "Wave energy converter: a review of wave energy conversion
        technology," in *2016 3rd Asia-Pacific World Congress on Computer Science and
        Engineering (APWC on CSE)*, 2016: IEEE, pp. 71-77.

[7]   T. Thorpe, "An overview of wave energy technologies: status, performance and
        costs," *Wave power: moving towards commercial viability,* vol. 26, pp. 50-120,
        1999.

[8]   H. Titah-Benbouzid and M. Benbouzid, "Ocean wave energy extraction: Up-to-
        date technologies review and evaluation," in *2014 International Power*

Electronics and Application Conference and Exposition, 5-8 Nov. 2014 2014, pp. 338-342, doi: 10.1109/PEAC.2014.7037878.

[9]   A. F. Falcão and J. C. Henriques, "Oscillating-water-column wave energy converters and air turbines: A review," *Renewable Energy,* vol. 85, pp. 1391-1424, 2016.

[10]   L. Margheritini, D. Vicinanza, and P. Frigaard, "SSG wave energy converter: Design, reliability and hydraulic performance of an innovative overtopping device," *Renewable Energy,* vol. 34, no. 5, pp. 1371-1380, 2009.

[11]   H. Kang and M. Kim, "Method and apparatus for wave energy conversion," ed: Google Patents, 2019.

[12]   C. Jin, H. Kang, M. Kim, and F. P. Bakti, "Performance evaluation of surface riding wave energy converter with linear electric generator," *Ocean Engineering,* vol. 218, p. 108141, 2020.

[13]   N. Hodgins, O. Keysan, A. S. McDonald, and M. A. Mueller, "Design and testing of a linear generator for wave-energy applications," *IEEE Transactions on Industrial Electronics,* vol. 59, no. 5, pp. 2094-2103, 2011.

[14]   E. Anderlini, D. I. Forehand, P. Stansell, Q. Xiao, and M. Abusara, "Control of a point absorber using reinforcement learning," *IEEE Transactions on Sustainable Energy,* vol. 7, no. 4, pp. 1681-1690, 2016.

[15]   P. Kracht, S. Perez-Becker, J.-B. Richard, and B. Fischer, "Performance improvement of a point absorber wave energy converter by application of an

observer-based control: Results from wave tank testing," *IEEE Transactions on Industry Applications,* vol. 51, no. 4, pp. 3426-3434, 2015.

[16]   E. Tedeschi and M. Molinas, "Tunable control strategy for wave energy converters with limited power takeoff rating," *IEEE Transactions on industrial electronics,* vol. 59, no. 10, pp. 3838-3846, 2011.

[17]   A. M. Alshawish, S. M. Eshtaiwi, A. Shojaeighadikolaei, A. Ghasemi, and R. Ahmadi, "Sensorless control for permanent magnet synchronous motor (PMSM) using a reduced order observer," in *2020 IEEE Kansas Power and Energy Conference (KPEC)*, 2020: IEEE, pp. 1-5.

[18]   S. Bolognani, R. Oboe, and M. Zigliotto, "Sensorless full-digital PMSM drive with EKF estimation of speed and rotor position," *IEEE transactions on Industrial Electronics,* vol. 46, no. 1, pp. 184-191, 1999.

[19]   H. A. Hussain and H. A. Toliyat, "Back-EMF based sensorless vector control of tubular PM linear motors," in *2015 IEEE International Electric Machines & Drives Conference (IEMDC)*, 2015: IEEE, pp. 878-883.

[20]   W. Zhao, S. Jiao, Q. Chen, D. Xu, and J. Ji, "Sensorless control of a linear permanent-magnet motor based on an improved disturbance observer," *IEEE Transactions on Industrial Electronics,* vol. 65, no. 12, pp. 9291-9300, 2018.

[21]   F. Naghavi, S. Sheshaprasad, M. Gardner, A. Meduri, H. Kang, and H. Toliyat, "Permanent Magnet Linear Generator Design for Surface Riding Wave Energy Converters," in *2021 IEEE Energy Conversion Congress and Exposition (ECCE)*, 2021: IEEE, pp. 4369-4375.

[22] National Oceanic and Atmospheric Administration [Online] Available:

https://www.ndbc.noaa.gov/station_history.php?station=41002

[23] L. Cappelli *et al.*, "Linear tubular permanent-magnet generators for the inertial sea wave energy converter," *IEEE Transactions on Industry Applications,* vol. 50, no. 3, pp. 1817-1828, 2013.

[24] L. Huang, M. Hu, Z. Chen, H. Yu, and C. Liu, "Research on a direct-drive wave energy converter using an outer-PM linear tubular generator," *IEEE Transactions on Magnetics,* vol. 53, no. 6, pp. 1-4, 2017.

[25] C. Liu, H. Yu, M. Hu, Q. Liu, and S. Zhou, "Detent force reduction in permanent magnet tubular linear generator for direct-driver wave energy conversion," *IEEE transactions on magnetics,* vol. 49, no. 5, pp. 1913-1916, 2013.

[26] A. Musolino, M. Raugi, R. Rizzo, and L. Sani, "A semi-anaytical model for the analysis of a permanent magnet tubular linear generator," *IEEE Transactions on Industry Applications,* vol. 54, no. 1, pp. 204-212, 2017.

[27] J. Prudell, M. Stoddard, E. Amon, T. K. Brekken, and A. Von Jouanne, "A permanent-magnet tubular linear generator for ocean wave energy conversion," *IEEE Transactions on Industry Applications,* vol. 46, no. 6, pp. 2392-2400, 2010.

[28] J. Wang, G. Jewell, and D. Howe, "Design optimisation and comparison of tubular permanent magnet machine topologies," *IEE Proceedings-Electric Power Applications,* vol. 148, no. 5, pp. 456-464, 2001.

[29]   J. Wang, G. W. Jewell, and D. Howe, "A general framework for the analysis and design of tubular linear permanent magnet machines," *IEEE Transactions on Magnetics,* vol. 35, no. 3, pp. 1986-2000, 1999.

[30]   J. Zhang, H. Yu, M. Hu, L. Huang, and T. Xia, "Research on a PM slotless linear generator based on magnet field analysis model for wave energy conversion," *IEEE Transactions on Magnetics,* vol. 53, no. 11, pp. 1-4, 2017.

[31]   S. Pakdelian, N. W. Frank, and H. A. Toliyat, "Principles of the trans-rotary magnetic gear," *IEEE transactions on magnetics,* vol. 49, no. 2, pp. 883-889, 2012.

APPENDIX A

Matlab codes for PTO simulation

1.   Passive Damping

```
1.    for indx = 1:(length(times)-1)
2.        speedsPassive(indx+1) = speedsPassive(indx) + timeStep*(-
9.81*(sin(angles(indx))/2+sin(angles(indx+1))/2)+forcesPassive(indx)/sl
idingMass);
3.
4.        positionsPassive(indx+1) = positionsPassive(indx) +
timeStep*0.5*(speedsPassive(indx) + speedsPassive(indx+1));
5.
6.        forcesPassive(indx+1) = -cPTO*speedsPassive(indx+1);
7.
8.        estimatedForcesPassive(indx+1) = -cPTO*speedsPassive(indx+1);
9.
if(abs(estimatedForcesPassive(indx+1))>min(maxForce,abs(maxPower/speeds
Passive(indx+1))))
10.           if(estimatedForcesPassive(indx+1)>0)
11.               forcesPassive(indx+1)=
min(maxForce,abs(maxPower/speedsPassive(indx+1)));
12.           else
13.               forcesPassive(indx+1)= -
min(maxForce,abs(maxPower/speedsPassive(indx+1)));
14.           end
15.       else
16.           forcesPassive(indx+1) = estimatedForcesPassive(indx+1);
17.       end
18.
19.       powersPassive(indx+1) = -
forcesPassive(indx+1)*speedsPassive(indx+1);
20.
21.    end
```

2.   Reactive Damping

```
1.    for indx = 1:(length(times)-1)
2.
3.        speedsReactive(indx+1) = speedsReactive(indx) + timeStep*(-
9.81*(sin(angles(indx))/2+sin(angles(indx+1))/2)+forcesReactive(indx)/s
lidingMass);
4.        positionsReactive(indx+1) = positionsReactive(indx) +
timeStep*0.5*(speedsReactive(indx) + speedsReactive(indx+1));
5.
6.        %Power and Force Limit on Reactive Damping
```

58

```
7.          estimatedForcesReactive(indx+1) = -
cPTO*speedsReactive(indx+1)-k*positionsReactive(indx+1);
8.
if(abs(estimatedForcesReactive(indx+1))>min(maxForce,abs(maxPower/speed
sReactive(indx+1))))
9.              if(estimatedForcesReactive(indx+1)>0)
10.                 forcesReactive(indx+1)=
min(maxForce,abs(maxPower/speedsReactive(indx+1)));
11.             else
12.                 forcesReactive(indx+1)= -
min(maxForce,abs(maxPower/speedsReactive(indx+1)));
13.             end
14.         else
15.             forcesReactive(indx+1) = estimatedForcesReactive(indx+1);
16.         end
17.             powersReactive(indx+1) = -
forcesReactive(indx+1)*speedsReactive(indx+1);
18.    end
```

3.   Binary Damping

```
1.     for indx = 1:(length(times)-1)
2.
3.         speedsBinary(indx+1) = speedsBinary(indx) + timeStep*(-
9.81*(sin(angles(indx))/2+sin(angles(indx+1))/2)+forcesBinary(indx)/sli
dingMass);
4.
5.         if speedsBinaryndx+1) < 0.01 && speedsBinary(indx+1) >= 0
6.             speedsBinary (indx+1) = 0.01;
7.         elseif speedsBinary (indx+1) > -0.01 && speedsBinary (indx+1)
<=0
8.             speedsBinary (indx+1) = -0.01;
9.         end
10.
11.        positionsBinary (indx+1) = positionsBinary (indx) +
timeStep*0.5*(speedsBinary (indx) + speedsBinary (indx+1));
12.
13.        % Binary Damping
14.        if speedsBinary (indx+1)> 0 && angles(indx+1)>0   ||
(speedsBinary (indx+1)> 0  && (slidingLength/2*factor - positionsBinary
(indx+1))/speedsBinary (indx+1) < speedsBinary
(indx+1)/(2*maxForce/slidingMass)) || (speedsBinary (indx+1)>0 &&
forcesBinary (indx+1) < 0 && (slidingLength/2*factor - positionsBinary
(indx+1))/speedsBinary (indx+1) < speedsBinary
(indx+1)/(2*maxForce/slidingMass))
15.
16.
```

```matlab
17.          if (speedsBinary (indx+1)>0 && forcesBinary (indx) < 0 &&
(slidingLength/2*factor - positionsBinary
(indx+1))/speedsBinary(indx+1) <
speedsBinary(indx+1)/(2*maxForce/slidingMass))
18.              dampingStatus1(indx+1) = 0.5;
19.
20.          elseif (speedsBinary(indx+1)>0  &&
(slidingLength/2*factor - positionsBinary(indx+1))/speedsBinary(indx+1)
< speedsBinary(indx+1)/(2*maxForce/slidingMass))
21.              dampingStatus1(indx+1) = 1;
22.          end
23.          forcesBinary(indx+1) = -
min(min(maxForce,abs(maxPower/speedsBinary(indx+1))),intertiaFactor*spe
edsBinary(indx+1)/timeStep*slidingMass);
24.
25.          powersBinary(indx+1) = forcesBinary(indx+1)*-
(speedsBinary(indx+1));
26.          dampingStatus(indx+1) = 0;
27.      elseif speedsBinary(indx+1)< 0 && angles(indx+1)<0   ||
(speedsBinary(indx+1)<0  && (-slidingLength/2*factor -
positionsBinary(indx+1))/speedsBinary(indx+1) < -
speedsBinary(indx+1)/(2*maxForce/slidingMass)) ||
(speedsBinary(indx+1)<0 && forcesBinary(indx+1) > 0 && (-
slidingLength/2*factor - positionsBinary(indx+1))/speedsBinary(indx+1)
< -speedsBinary(indx+1)/(2*maxForce/slidingMass))
28.
29.
30.          if (speedsBinary(indx+1)<0 && forcesBinary(indx) > 0 &&
(-slidingLength/2*factor -
positionsBinary(indx+1))/speedsBinary(indx+1) < -
speedsBinary(indx+1)/(2*maxForce/slidingMass))
31.              dampingStatus1(indx+1) = 0.5;
32.
33.          elseif (speedsBinary(indx+1)<0  && (-
slidingLength/2*factor - positionsBinary(indx+1))/speedsBinary(indx+1)
< -speedsBinary(indx+1)/(2*maxForce/slidingMass))
34.              dampingStatus1(indx+1) = 1;
35.          end
36.
37.          forcesBinary(indx+1) =
min(min(maxForce,abs(maxPower/speedsBinary(indx+1))),-
intertiaFactor*speedsBinary(indx+1)/timeStep*slidingMass);
38.
39.          powersBinary(indx+1) = forcesBinary(indx+1)*-
(speedsBinary(indx+1));
40.          dampingStatus(indx+1) = 0;
41.      end
42.  end
```

1. Binary-reactive Damping

```
1.    for indx = 1:(length(times)-1)
2.
3.        speedsBinaryReactive(indx+1) = speedsBinaryReactive(indx) +
timeStep*(-
9.81*(sin(angles(indx))/2+sin(angles(indx+1))/2)+forcesBinaryReactive(i
ndx)/slidingMass);
4.
5.        if speedsBinaryReactive(indx+1) < 0.01 &&
speedsBinaryReactive(indx+1) >= 0
6.            speedsBinaryReactive(indx+1) = 0.01;
7.        elseif speedsBinaryReactive(indx+1) > -0.01 &&
speedsBinaryReactive(indx+1) <=0
8.            speedsBinaryReactive(indx+1) = -0.01;
9.        end
10.
11.       positionsBinaryReactive(indx+1) =
positionsBinaryReactive(indx) +
timeStep*0.5*(speedsBinaryReactive(indx) +
speedsBinaryReactive(indx+1));
12.
13.       % Binary Damping
14.       if speedsBinaryReactive(indx+1)> 0 && angles(indx+1)>0  ||
(speedsBinaryReactive(indx+1)> 0  && (slidingLength/2*factor -
positionsBinaryReactive(indx+1))/speedsBinaryReactive(indx+1) <
speedsBinaryReactive(indx+1)/(2*maxForce/slidingMass)) ||
(speedsBinaryReactive(indx+1)>0 && forcesBinaryReactive(indx+1) < 0 &&
(slidingLength/2*factor -
positionsBinaryReactive(indx+1))/speedsBinaryReactive(indx+1) <
speedsBinaryReactive(indx+1)/(2*maxForce/slidingMass))
15.
16.
17.           if (speedsBinaryReactive(indx+1)>0 &&
forcesBinaryReactive(indx) < 0 && (slidingLength/2*factor -
positionsBinaryReactive(indx+1))/speedsBinaryReactive(indx+1) <
speedsBinaryReactive(indx+1)/(2*maxForce/slidingMass))
18.               dampingStatus1(indx+1) = 0.5;
19.
20.           elseif (speedsBinaryReactive(indx+1)>0  &&
(slidingLength/2*factor -
positionsBinaryReactive(indx+1))/speedsBinaryReactive(indx+1) <
speedsBinaryReactive(indx+1)/(2*maxForce/slidingMass))
21.               dampingStatus1(indx+1) = 1;
22.           end
23.           forcesBinaryReactive(indx+1) = -
min(min(maxForce,abs(maxPower/speedsBinaryReactive(indx+1))),intertiaFa
ctor*speedsBinaryReactive(indx+1)/timeStep*slidingMass);
24.
```

```matlab
25.           powersBinaryReactive(indx+1) =
forcesBinaryReactive(indx+1)*-(speedsBinaryReactive(indx+1));
26.           dampingStatus(indx+1) = 0;
27.       elseif speedsBinaryReactive(indx+1)< 0 && angles(indx+1)<0
|| (speedsBinaryReactive(indx+1)<0  && (-slidingLength/2*factor -
positionsBinaryReactive(indx+1))/speedsBinaryReactive(indx+1) < -
speedsBinaryReactive(indx+1)/(2*maxForce/slidingMass)) ||
(speedsBinaryReactive(indx+1)<0 && forcesBinaryReactive(indx+1) > 0 &&
(-slidingLength/2*factor -
positionsBinaryReactive(indx+1))/speedsBinaryReactive(indx+1) < -
speedsBinaryReactive(indx+1)/(2*maxForce/slidingMass))
28.
29.
30.           if (speedsBinaryReactive(indx+1)<0 &&
forcesBinaryReactive(indx) > 0 && (-slidingLength/2*factor -
positionsBinaryReactive(indx+1))/speedsBinaryReactive(indx+1) < -
speedsBinaryReactive(indx+1)/(2*maxForce/slidingMass))
31.               dampingStatus1(indx+1) = 0.5;
32.
33.           elseif (speedsBinaryReactive(indx+1)<0  && (-
slidingLength/2*factor -
positionsBinaryReactive(indx+1))/speedsBinaryReactive(indx+1) < -
speedsBinaryReactive(indx+1)/(2*maxForce/slidingMass))
34.               dampingStatus1(indx+1) = 1;
35.           end
36.
37.           forcesBinaryReactive(indx+1) =
min(min(maxForce,abs(maxPower/speedsBinaryReactive(indx+1))),-
intertiaFactor*speedsBinaryReactive(indx+1)/timeStep*slidingMass);
38.
39.           powersBinaryReactive(indx+1) =
forcesBinaryReactive(indx+1)*-(speedsBinaryReactive(indx+1));
40.           dampingStatus(indx+1) = 0;
41.
42.       % Reactive Damping
43.       else
44.         estimatedForcesBinaryReactive(indx+1) = -
cPTO*speedsBinaryReactive(indx+1)-k*positionsBinaryReactive(indx+1);
45.
if(abs(estimatedForcesBinaryReactive(indx+1))>min(maxForce,abs(maxPower
/speedsBinaryReactive(indx+1))))
46.               if(estimatedForcesBinaryReactive(indx+1)>0)
47.                   forcesBinaryReactive(indx+1)=
min(maxForce,abs(maxPower/speedsBinaryReactive(indx+1)));
48.               else
49.                   forcesBinaryReactive(indx+1)= -
min(maxForce,abs(maxPower/speedsBinaryReactive(indx+1)));
50.               end
51.           else
```

```matlab
52.             forcesBinaryReactive(indx+1) =
estimatedForcesBinaryReactive(indx+1);
53.         end
54.             powersBinaryReactive(indx+1) = -
forcesBinaryReactive(indx+1)*speedsBinaryReactive(indx+1);
55.             dampingStatus(indx+1) = 1;
56.
57.     end
58.
59.   end
```